This preprint is now in press at: http://novapublishers.com/catalog/product_info.php?products_id=2176

Revised Draft 1 May 2004

Electron and Positive Ion Beams and X-rays Produced by Heated and Cooled Pyroelectric Crystals such as $LiNbO_3$ and $LiTaO_3$ in Dilute Gases: Phenomenology and Applications

James D. Brownridge
Department of Physics, Applied Physics and Astronomy, State University of New York at Binghamton, P.O. Box 6000, Binghamton, New York 13902-6000, e-mail jdbjdb@binghamton.edu

Stephen M. Shafroth
Department of Physics and Astronomy, University of North Carolina at Chapel Hill, Chapel Hill, North Carolina 27599-3255, e-mail shafroth@physics.unc.edu

Abstract

A systematic study has been undertaken of the phenomena associated with the acceleration of nearly monoenergetic high-energy electron and positive ions away from and towards the crystallographic z surfaces of crystals of $LiNbO_3$ and $LiTaO_3$ when they are heated and cooled in a dilute gas. Electron spectra show a multiple peak behavior i.e. peaks of energy E, 2E, 3E are detected. Current vs. time and temperature produced by heated pyroelectric crystals in dilute gas is reported as well as the relationship to x-ray emission… Gas amplification of electron beam energy is described. When the -z surface of a crystal is exposed in dilute gas and the crystal is cooling a self-focusing electron beam is accelerated away from the vicinity of the -z surface. When the +z surface of a crystal is exposed and the crystal in cooling a self-focusing electron beam is accelerated towards the crystal. Conversely when the -z surface of a crystal is exposed and the temperature is raising a self-focusing positive ion beam is accelerated away from the vicinity of the crystal and on cooling the positive ion beam is believed to be accelerated towards the crystal. Self-focused electron beams with energies as high as 170 keV and self-focused positive ion beam with energies as high as 113 keV have been observed. Low temperature behavior of $LiNbO_3$ and LiTaO3 are described and the temperatures where the pyroelectric coefficient goes to zero are reported as 14.09 ± 0.05K and 11.384 ± 0.011K respectively. High temperature behavior up to 200 ^oC and above where $LiNbO_3$ becomes conducting is reported. The pyroelectric crystals produce high electric fields and the behavior in dilute gases is explained qualitatively. New uses of pyroelectric crystal x-ray generators as portable bremsstrahlung photon fluorescence devices for K x-ray production of high Z up to Bi are described as well as use in teaching x-ray and beam physics. Pyroelectric crystal electron accelerators have been used to excite characteristic K x-rays from tree leaves through out the growing season. Future prospects for pyroelectric crystal research are discussed.

Introduction

It is the intent of this paper to summarize what is known about the phenomena that leads to self-focusing electron and positive ion beams and the production of x rays when a pyroelectric crystal of $LiNbO_3$ or $LiTaO_3$ is slowly heated and cooled in dilute gases. We will present a phenomenological discussion of the many phenomena that have been reported and in particular those that we have observed in our laboratories. No comprehensive theory has yet been developed that explains all of these phenomena, therefore, we will not address them individually or collective from a theoretical point of view. We will present and discuss experimental data and observations that have lead to our understanding of many of these phenomena. The experimental data and observations that we discuss here were all performed and observed in our laboratories. Many have been confirmed in other laboratories but have not yet appeared in the referred literature.[34] Others have been reported on from time to time at conferences and in journal publications by us, however, there are many new systematic studies, interpretations and observations in this paper.

There is voluminous literature on all sorts phenomena associated with pyroelectric crystals from ancient Greek and Roman times (315 B. C.)[1] to the present. In 1972 the idea was put forward that pyroelectric crystals could be used to generate x rays.[2] In 1992 the first fully operational Crystal X-Ray Generator was developed by one of us (JDB).[3] In 2003 Amptek, Inc introduced a commercial produced, the Cool X X-Ray Generator.[4] With this long history there is still much to be learned about these crystals and except for the 1972 patent, prior to our work in 1992 we have not been able to find in the refereed literature a discussion of x ray production by pyroelectric crystals during slow heating and cooling of the crystals.

Electron emission from ferroelectrics (FEE) both "strong" and "weak" covers a wide area and is discussed widely in the literature[5]. The generic term "electron emission" should not be confused with or applied to the pyroelectric phenomena that give rise to focused beams of electrons, positive ions and crystal x-ray generators that we will discuss. The phenomena of interest here do not involve a polarization reversal, an application of a high-voltage pulse, a fast heat pulse or mechanical pressure to cause electron emission. Very few if any of the electrons or ions we are observing are emitted out of the surface of the crystal. The majority of the electrons and ions described here are thought to be due to field ionization via tunneling of electrons from residual gas molecule near the crystal surface and these are the electrons and ions that are focused and accelerated by the electric fields that are produced when the temperature of the crystal is slowly changed. We need only change the temperature of a pyroelectric crystal in a dilute gas to produce most of the effects that will be discussed here. For a discussion of the broad topic of "electron emission from ferroelectrics" we suggest reference 5 a recent (December 2000) review article and the references therein. However, self-focused beams of ions, electrons and crystal x-ray generators are not discussed in this review article. These are recent developments.

Some low temperature measurements are described which show a new phenomenon; the fact that the pyroelectric coefficient goes to zero in the neighborhood of 10 K for both $LiNbO_3$ and $LiTaO_3$.

Brief History of Pyroelectric Crystals

Pyroelectric crystals such as kidney stones of lynx as well as amber have been known at least since ancient Greek and probably as far back as biblical times. They were found to have the power to attract straws, bits of wood and even metals. When heated by sunlight or other means. Their primary interest was for medicinal purposes but they also attracted attention for their "magical" properties. After about two thousand years when the scientific revolution was in full bloom, interest in these crystals suddenly grew. Their electrical properties were compared with the magnetic properties of lodestone. A Dutch scientist, Franz Aepinus in 1756 listed what he called the five laws of the electricity of tourmaline. He starts by saying that a tourmaline crystal always has positive and negative electricity. He then goes on to say that if the crystal is heated one always finds that one face is positive and the other negative. Tourmaline becomes electrified when rubbed. It is interesting to note that a controversy developed over the behavior of pyroelectric crystals and in 1759 one was given to Benjamin Franklin, who did some experimenting with the tourmaline crystal and concluded that Aepinus was right. Then in 1759 John Canton was the first to observe that the electrical polarity of tourmaline was reversed on cooling. Other distinguished scientists who worked on pyroelectricity during the eighteenth century were the Englishman Joseph Priestly and the French Count de Buffon.

In the nineteenth century much work was done to gain further insight into the properties of pyroelectric crystals. Notably Jean-Mothee Gaugain reached the following conclusions, which form the basis of our present day thermodynamic interpretation of pyroelectric crystals.

1. The total quantity of electricity produced by a crystal of tourmaline depends uniquely on the limits within which its temperature is changed.
2. Within the same temperature limits, the quantity of electricity produced during heating is the same as that produced during cooling, but the signs of the charges are reversed
3. The quantity of charge produced is proportional to the cross-sectional area and is independent of its length.

The first major theoretical treatments of pyroelectricity were published by Lord Kelvin in 1878 and 1893. The thermodynamic connection between temperature, electric field and mechanical stress is shown in a diagram after J. F. Nye[6] and is shown in Fig. 1.

X-ray and Electron Production by Pyroelectric Crystals

In 1972 a patent[2] was issued for an "Electron and X-Ray Generator" that would produce electrons and x rays by heating a pyroelectric crystal from 25 ^{o}C to 100 ^{o}C. To the best of our knowledge the first working model that produced x rays with enough energy and intensity to be useful in teaching and research was not produced until 1992.[3] Then in 1999 Brownridge and Raboy wrote a comprehensive paper[7] describing the x-ray emission and light production in the plasma [5,7,9] around the crystal for several different crystals and gases. Also in 1999 Shafroth et. al. studied the time dependence of x-ray emission.[10] Further they studied the effect on total x-ray yield for five different gases and found a marked decrease in yield for O_2, which was due to the production of ozone in the plasma. Also in 1999 Shafroth and Brownridge reported on the use of pyroelectric crystals in the teaching of x-ray physics[11]. Then in 2001 Brownridge and et. al. reported on the production of nearly monoenergetic electrons by pyroelectric crystals in dilute gases.[12] Before 1992[3] it was assumed[2,5,13] that electrons were coming out of the crystals and that they would have to be replaced between thermal cycles. This turned out to be an incorrect assumption and may have lead to the delay in the development of this technogoly.

The proposal for electron replenishment was to connect the backside of the crystal and the target to a common ground[2]. This could not possible work because the electrical conductivity in these crystals is far too low to permit electron transport at the suggested operating temperature of 25 ^{o}C to 100 ^{o}C.[14] In 1992 we realized that the source[3] of the electrons reportedly emanating "from" the crystal may in fact arise from the gas around the crystal. Furthermore, it was later discovered[15] that both electrons and positive ions were accelerated away from the vicinity of the surface of these crystal in focused beams and that nothing needed to be grounded for the system to work indefinitely, just cycle the temperature of the crystal in a dilute gas and maintain a stable pressure.

In order to bring clarity to the question of the source of the electrons that many researchers[16,17,18,19,31,32] reported observing when pryoelectric crystals are heated and cooled in a vacuum, a series of experiments was undertaken which demonstrated that electrons did not come out of the crystal during a slow change of temperature.[7] Further experiments that will be described below were all done to elicited additional information about the sources of ions and electrons at a pressure of 0.1 mTorr. The inset in figures shows the experimental arrangement used to acquire these data graphed in these figures. In Fig. 2 we show charge build up on the -z base of a $LiNbO_3$ crystal as the temperature is raised in steps. The -z base was covered with silver epoxy, which in turn is connected to an electrometer. The electrometer is in the charge mode. The +z base was also covered with silver epoxy, which is in contact with an electrical insulator that is part of the heater. In this arrangement charge cannot escape the -z base/electrometer system except by leakage to the environment or through the crystal to the +z base, there are no paths to ground. It is evident that there was minimal if any loss of charge from the -z surface of the crystal below about 200 ^{o}C. Above about 280 ^{o}C there was a precipitous loss of charge from the -z base. Raising the temperature above 200 ^{o}C lowers the electrical

resistivity enough for charge to migrate through the crystal while the polarization continues to decrease leaving even more charge uncompensated for by polarization charge. The increasing charge measured at the start of increasing temperature was charge held at the surface of the crystal by polarization charge and then released when the temperature began rising and polarization began to decrease. Below about 200 ^{o}C there was no escape for this freed surface charge and it builds up. When the temperature of the crystal is cycled between two temperatures below 200 ^{o}C as is shown in Fig. 3, the surface charge will increase and decrease with the temperature showing no net loss or gain in surface charge. There is no charge transport through the crystal. In Fig. 4 we switched the electrometer to the ammeter mode and repeated the experiment of increasing the temperature of the crystal in steps. Here we saw a current flowing between the –z base of the crystal and ground through the ammeter following each increase in temperature. This is charge that was held on the surface of the crystal by polarization charge.

Next the silver epoxy covered crystal is replaced with one whose –z base is exposed and is ~1cm away from a ~1cm^2 metal target as shown in the inset in Fig. 5. The target foil is connected to the ammeter as in the previous experiments. Again the temperature of the crystal is raised in steps. This time instead of measuring a current when the ammeter probe was in direct contact with the crystal, now the ammeter probe was at a distance of 1cm in a vacuum of ~0.1 mTorr. An x-ray detector was positioned to detect x rays if they were produced at energies above the threshold of the detector when electrons strike the crystal or the target during temperature changes. In Fig. 5 the temperature was raised from ~25 ^{o}C to ~70 ^{o}C just as it was in step one in Fig. 4 and the ammeter response was about the same as it was to the first step in temperature increase in Fig. 4. A current flowed between the –z base of the crystal and ground through the ammeter while the temperature was changing. No x rays were produced because under these circumstances a change in temperature of 45 ^{o}C did not produce a sufficiently high voltage at the surface of the crystal to accelerate electrons to the necessary energy. In Fig. 6 the temperature was raised from ~25 ^{o}C to ~130 ^{o}C. This time the picoammeter response is quite different. Instead of one rise and fall of current in response to a smooth continuous increase in temperature we see a second rise in the current as the temperature passes through ~80 ^{o}C ten degrees higher than the maximum in Fig. 5. This second rise in current coincided with the onset of x ray production. The same phenomenon is observed during cooling as the temperature falls through ~ 90 ^{o}C. The two temperatures are not unique to this crystal; they are primarily a function of pressure, geometry and the heating and cooling rates. The second increase in current is due to x ray ionization of residual gas molecules. During increasing temperature electron are accelerated to the crystal and produce characteristic x rays of elements in and on the surface of the crystal.[7] During cooling electron are accelerated away from the crystal and strike the target producing characteristic x rays of elements in the target. In both cases these x-rays produce secondary ionization within the system thereby increasing the current through the ammeter. Rotating the crystal 180^{o} will produce a similar results with the current reversed.

With this new information it was possible to build a variety of useful crystal x-ray generators.[4,10,12,15,20] In Fig. 7 we show one of our earliest models, it is all glass except for the wire leads to the lamp/heater. This design clearly demonstrated that that electron were not coming out of the crystal and therefore did not have to be replaced. Increase or decrease the pressure in the glass tube and the electron fluence increase and decreased. The source of the electrons was the gas surrounding the crystal.

Low Temperature behavior of Pyroelectric Crystals

When the temperature of a pyroelectric crystal falls to below the Curie temperature it is spontaneously polarized. The absolute magnitude of the polarization increases with decreasing temperature but the pyroelectric coefficient decreases. The absolute magnitude of the polarization decreases with rising temperature and the pyroelectric coefficient increases as long as the crystals is below the Curie temperature and above the "polarization saturation temperature", see Fig. 8. The "polarization saturation temperature" is the temperature below which the polarization does not change with temperature. It is also the temperature at which the pyroelectric coefficient $P = \Delta Q/\Delta T \cdot A$ is 0. This implies that the crystal structure is no longer anisotropic. For $LiNbO_3$ it is 14.09± 0.05K and for $LiTaO_3$ it is 11.384± 0.011K [21]. The curie temperature[22,23] for $LiNbO_3$ is 1210^{o}C and 685^{o}C for $LiTaO_3$. Above the Curie temperature these pyroelectric crystals are in the paraelectric phase and are therefore electrically neutral. Below the Curie temperature these crystals are in the ferroelectric phase and are polarized, therefore, their polar ends are electrically charged. The polarization is manifested by the presence of an electric field external to the crystal during temperature changes. If a sufficient length of time has elapsed since a change in temperature the polarization charge will be neutralized by free charge attracted to the surface of the crystal from the environment. We see no evidence of charge migration through these crystals at temperatures below about 200 ^{o}C.[14] Once neutralization is complete one can no longer detect the presence of an electric field external to the crystal. Yet the polarization has not changed.

How Pyroelectric Crystals Produce High Electric Fields

Uncompensated charge in or on the surface of these crystals is the source of the high electric fields produced by these crystals. Changing the temperature of a $LiNbO_3$ crystal from 25 ^{o}C to 100 ^{o}C in a very short time compared to polarization charge neutralization time will result in a spontaneous polarization change ΔP_s of 0.015 C/m^2. The strength of electric field on the surface of the crystal will be $|E_0| = 1.35 \times 10^7$ V/cm[13, 18]. This is strong enough to ionize gas molecules that approach the surface of the crystal.[19,24,25] Over time $|E_0|$ will decrease to zero as the polarization change is compensated by charge from the environment.

The crystallographic structure of $LiNbO_3$ and/or $LiTaO_3$ is quite similar and we show an abbreviated diagram of a unit cell in Fig. 9. A full discussion of the crystallographic structure of $LiNbO_3$ and $LiTaO_3$ can be found in references 22 and 26.

In Fig. 9(a) we show the positions of the Li, Nb and/or Ta atoms relative to the planes of the oxygen atoms. Here the crystal is above the Curie temperature in the paraelectric phase, notice that the Li ions lie in the plane of an oxygen layer and the Nb and/or Ta ions are centered statically between the planes of two oxygen layers. In Fig. 9(b) we show the position of the Li and Nb or Ta ions in the crystal after it is cooled to a temperature below the Curie temperature into the ferroelectric phase, here the Li ion has moved out of the plane of the oxygen atoms and towards the +z end of the crystal along the z-axis. Likewise the Nb and/or Ta atoms have moved away from the center of the two-oxygen layers and towards the +z end of the crystal. This movement is caused by the decrease in temperature. Movement of these atoms with respect to the oxygen atoms is what gives rise to the spontaneous polarization. The +z end of the crystal becomes more positively charged and the -z end of the crystal becomes more negatively charged with decreasing temperature. If the temperature is raised the polarization decreases as the Li and Nb or Ta atoms move back towards their position when the crystal is in the paraelectric phase. The charge that appears at the ends of these crystals is called "polarization charge" and is fixed in the surface of the crystal. This charge does not leave the surface of these crystals and there is minimal or no migration through the crystal as long as the temperature is below about 200 ^{o}C. Above about 200 ^{o}C the resistivity is low enough for charge to begin migrating through the crystal, see Fig. 2. The lack of migration of charge through these crystals is the key property that makes these two crystals good electron and ion accelerators at temperatures below about 200 ^{o}C and above the "polarization saturation temperature".

In an environment where free charge is readily available, i.e. in room air at 1 atm, the spontaneous polarization charge that appears at the surface of a pyroelectric crystal, is quickly masked by charge attracted to the surface of the crystal from the room air. Therefore, within a very short time after a change in temperature in either direction there is little if any manifestation of an electric field associated with the increase or decrease in polarization of the crystal. The new polarization charge will have been neutralized by the acquisition of external electrical charge on the surface of the crystal. However, if the crystal is in a vacuum or in a reduced pressure environment where there is a limit on the amount of free electrical charge and gas molecules that can be ionization to produce free electrical charge an electric field external to the crystal will be present for a considerable time. The electric field is produced by uncompensated polarization charge in the surface of the crystal as illustrated in Fig. 10. Polarization charge in the surface is compensated by charge attracted to the surface from the external environment. The strength of the field is determined by the gas pressure around the crystal, the net change in temperature and the elapsed time following the temperature change. The gas surrounding the crystal is the source of electrical charge that neutralizes the polarization charge as the temperature of the crystal changes. If the gas pressure is high (1 atm) then polarization charge will be neutralized almost as fast it appears in the surface of the crystal. On the other hand, if the gas pressure is low ($<10^{-6}$ torr) then there will not enough gas to provide charge at a rate equal to the rate of polarization charge production, consequently, uncompensated charge will appear in the surface of the crystal. Once the temperature of a crystal become stable the polarization charge in its surface will be compensated/neutralized at a rate determined primarily by the number of gas molecules in the vacuum around the crystal and the

temperature of the gas. In effect the rate of neutralization is determined by the rate at which gas molecules randomly come close enough to the surface of the crystal to be ionized by the electric field at the surface of the crystal. If the surface is negatively charged then the positive ion is electrically held at the surface of the crystal and the electron is accelerated away. A typical electron spectrum is shown in Fig. 11. If the surface is positive then the electron is held and the ion is accelerated away. A typical positive ions spectrum is shown in Fig. 12. The energy to which electrons are accelerated too is determined by the uncompensated polarization charge present when ionization takes place plus a factor we call "gas multiplication", which will be discussed later. The energy to which positive ions are accelerated too is determined only by the uncompensated polarization charge present when ionization occurs.

Nearly Monoenergetic Electron Production

Nearly monoenergetic electron production is another one of the phenomena observed during a slow thermal cycling of a pyroelectric crystal in a dilute gas that is not yet well understood. However, we believe we have learned enough to discuss a possible mechanism. This discussion will deal with the case where -z base is exposed and cooling in nearly ideal conditions. The pressure is $<8X10^{-7}$ Torr. We will neglect gas amplification although it is always presence because of the lack of an ideal vacuum. In an ideal vacuum there would be no gas molecules to ionize, hence no electrons to accelerate and detect. This argument will also apply when the +z base is exposed as is shown in Fig. 13($T_{2'}$), however, the temperature will need to be rising. In the +z case the electric field is due electrons on the surface of the crystal. Not internal polarization charge. We referred to these electrons as compensation charge. As we have discussed earlier when the crystal is cooling the -z base becomes increasingly negatively charge due to increasing polarization charge in the surface of the crystal.[27]

If the crystal is at a stable temperature below the Cutie point (Fig. 13(T_2) and all polarization charges are compensated for before the onset of further cooling, the electric field strength external to the crystal will be zero. As the crystal begins cooling the electric field becomes non-zero (Fig. 13(T_3)) due to the increasing negative uncompensated polarization charge. At any instant in time the electric field strength at any point external to the crystal is proportional to the total uncompensated polarization charges and the distance of that point from the surface of the crystal, we are neglecting gas amplification. Neutral gas molecule are randomently moving about the system and regulatory approaches close enough to the crystal to be ionized by the electric field that originates at the surface of the crystal. Neutral gas molecules in this electrical field will be ionized when they arrive at a point where the field is strong enough to completely remove an electron. Since the strength of the electric field is not uniform and decreases with distance from the surface of the crystal there is a unique distance i.e. < 1 μ from the surface that a molecule must arrive at to be ionized. At this distance the electric field strength is unique and an electron that is removed from a gas molecule at this point will have a unique energy when it arrives at the detector. Keeping in mind that the uncompensated polarization charge is continuously changing, therefore the strength of the electric field

and distance from the crystal surface that a molecule must arrive at is also changing. The net results is that if one measure the energy of electrons accelerated away from the crystal at any instance in time they will all have approximately the same energy. There is a spread in the measured electron energy because of the spread in distance from the crystal from which they originate. It takes a finite amount of time to collect each spectrum but this is not the source of the peak width. At instant of time all electrons will have approximately the same energy. In Fig. 14 we show electrons energy and crystal temperatures at several instances in time (10 sec) as the crystal cools in a vacuum of $<8X10^{-7}$ Torr. Since we measured the electrons energy in less than ideal conditions not all electrons arriving at the detector have the exact same energy. Scattering and other effect account for this, Fig. 15 is an example of an electron energy spectrum collected at an instance in time during cooling between T_2 and T_3 in Fig. 13. Although we neglected gas amplification during this argument it is always present and varies with pressure. We show in Fig. 16 electrons energies and crystal temperatures at several instance in time as the crystal cools in a vacuum of $\sim 10^{-3}$ Torr to illustrate this point.

The multiple peaks shown in Figs. 11, 15 and 35 are the results of 1, 2, 3 and etc. electrons arriving at the detector within the resolving time of the electronics. Peak 2 is twice the energy of peak 1 and peak 3 is three times the energy peak 1 and etc. The probability of more than one electron arriving at the detector within the resolving time is greatly increased by the self-focusing phenomenon that we will discussed later. When the system is perturbed in any number of ways multiple peaks production may be interrupted or the peaks shapes distorted during the perturbation. An example of this is shown in Fig. 17. Here changing pressure destabilizes the self-focusing. A photograph of this type of instability is shown in Fig. 23 where the spot is enlarged due to slowly rising pressure. In this situation fewer electrons pass through the slit and into the detector within the resolving time of the electronics even though in some cases the overall electron count rate may increase.

We will now discuss a phenomenon for which we are not prepared to offer a detail explanation. We will use the term "splitting" to denote that two peaks appear in the electron spectra where previously there was one. The phenomenon is transient and does not last the entire cool down cycle. It is most dramatic when cooling is continued below 20 ^{o}C. On rare occasions we have observed this phenomenon above 20 ^{o}C. In Fig. 18 we show a series of electron spectra taken as snapshots as the crystal cools through 30 ^{o}C on the way to -25 ^{o}C. The crystal was heated to the usual to 170 ^{o}C, we began taking snapshot spectra at 100 ^{o}C as was usual. The pressure was $< 10^{-7}$ Torr and the gas was N_2. The crystal was $LiNbO_3$ 4 mm diameter and 10 mm long. The distance was 22 mm. In Fig. 19 we show a spectrum where the "splitting" is clearly seen in every peak. Peak 1 is not resolved nevertheless, "splitting" is evident. If our assumptions and speculations about the production of multiple electron peaks are correct then these data suggest that at some point during cooling conditions developed such that there are two locations near the surface of the crystal where neutral gas molecules are ionized. This phenomenon warrants further study.

Focused electron and positive ion beams

Spatially stable self-focusing electron and positive ion beams have been produced by cylindrical pyroelectric crystals of $LiNbO_3$ and $LiTaO_3$.[15] Here our discussion will center on electron beam production when electrons are accelerated away from the -z base of the crystal, however, if the crystal is rotated 180 degrees these comments will also apply and the beam will be a positive ion beam. The source of electrons and ions that make up the beams are from the residual gas molecules that surround the crystal in the vacuum system that houses the crystal. The type of gas is not important. Molecules are ionized by the high electric field produced by the crystal when there is a change in the temperature of the crystal. In the specific case, to be discussed here the gas was room-air. The –z base end of a 4mm diameter by 10mm long $LiNbO_3$ was exposed as shown in Fig. 20.

The pressure in the chamber ranged from 10^{-6} Torr to about 10 mTorr. Heat was applied to the +z base end of the crystal that was epoxied to a 62-ohm resistor, the heater. The crystal was heated from about 20^{o}C to about 115 ^{o}C then allowed to cool back to about 20 ^{o}C. As it cooled a self-focusing spatially stable electron beam was produced. In Fig. 21 we image the beam by placing a ZnS screen at the focal length of the crystal, for this crystal the focal length was 22mm. That is the point where the electron beam image is smallest when the screen is perpendicular to the z-axis and moved back and forth along a line running through the center of the of the crystal.

The beam becomes spatially stable typically when the temperature falls below about 50 ^{o}C and may remain both focused and stable for many hours after the crystal has returned to about 20 ^{o}C if the pressure is in the range of 10^{-6} torr, see Fig 22. For pressures in the range of 10^{-3} Torr the beam may only last for several minutes and at a slightly higher pressure it will not stabilize or focus well, (see Fig. 23) at yet higher pressures (8-10 mTorr) the forming beam will "blow up", as shown in Fig. 24, a runway ionization of the gas around the crystal. When this happens all of the polarization charge on the surface of the crystal in compensated for or neutralized at the instance of "runway ionization" and the external field drops to zero. The electric field will again begin to increase as cooling continues.

The key to the production of the highest beam intensity is to maximize gas pressure and cooling rate (polarization charge production) to just below the "runway ionization" threshold. That is, we do not want the electric field strength to build to the breakdown point for the pressure we have selected. Since the amount of polarization charge is finite for a given temperature change and the polarization charge compensation rate is pressure dependent we can avoid "runway ionization" by the selection of a cooling rate, that will ensure that the electric field does not exceed the breakdown point and trigger runway ionization. We find it easer to vary the pressure and allow the cooling to occur naturally. The pressure limit will vary with the geometry of the vacuum chamber. In general the smaller the vacuum chamber the higher the pressure before runway ionization. The size of the vacuum chamber is shown in Fig. 20. The dimensions, 45 cm long and 7.5 cm in diameter.

In a low pressure environment (10^{-6} Torr) the cool-down rate is less important because the gas breakdown point is much higher. However, beam intensity is low because the number of gas molecules available to be ionized is also down. In other words the average time between gas molecules being ionized is longer.

Each time a gas molecule is ionized the positive ion is attracted to and sticks to the crystal, this positive ion compensates for one negative polarization charge thereby reducing the electric field external to the crystal by an amount equivalent to one unit of negative polarization charge. At the same time the freed electron is accelerated away from the -z base of the crystal by the electric field produced by the remaining uncompensated negative polarization charges. The direction is towards a point a fixed distance in front of the crystal. We call the distance to this point the focal length. It appears that the focal length is determined by the geometry of the crystal, primarily the diameter and length of the crystal. Temperature and pressure do not seem to play a roll in determining the focal length. However, pressure does affect the sharpness of the focusing as can be seen when the image in Fig. 23 is compared with the image in Fig. 21.

Simultaneously as electrons are being accelerated away from the crystal positive ions are being accelerated towards the crystal. And when positive ions are being accelerated away electrons are being accelerated towards the crystal. In both cases we believe that the ions and electrons are focused. When focusing was away from the crystal we were able to profile the beam by measuring the relative concentration of ions or electrons at various distances from the crystal, see Figs. 25 and 26. The electron beam was also imaged at its focal point, see Fig. 21. For positive ions or electrons accelerated towards the crystal it was not possible to profile relative concentration. However, it was possible to image the location on the surface of the crystal where electrons struck the crystal. To facilitate this the +z base of the crystal was coated with a thin layer of ZnS; this allowed us to image the spot where electrons struck the crystal. During most of the cooling with the +z based exposed as shown in Fig. 27(a) and (b) there was a bright spot near the center of the crystal that first grows in intensity then began fading as the crystal approached room temperature, Fig. 27(c). Near room temperature the spot diffused out over the surface of the crystal and the whole surface dimly fluoresce with varying intensity. Photographs of the fluorescent spot where electrons struck the crystal are shown in Fig. 28. Here a small magnet deflects the self-focused electron beam. The arrow in each frame points to the approximate location of the magnet. With no magnet near by the spot remain stable near the center of the crystal for most of the cool down once it self-focuses. The crystal was heated and then allowed to cool as usual in a dilute gas. We have not been successful in imagining the positive ion beam.

It is not fully understood why electron and positive ions are focused and why each crystal has a unique focal length when they are accelerated away from the crystal but it may be related to plasma focusing. In Fig. 25 we show cartoons of the electron beam inferred from the data presented in Figs. 26, 29 and 30. The dynamical behavior of the electron beam with pressure is illustrated in a video clip in reference 29. We have not observed isotropic distribution in the spatial angel 2π as reported in reference 32.

Gas Amplification of Electron Energy

Gas amplification of electron energy is a counter intuitive phenomenon that occurs when the gas pressure surrounding the pyroelectric crystal is increased.[20] Usually, when an electron is moving through a gas and the gas pressure is increased it loses energy to the gas. Here we describe a process by which electrons moving through gas gain energy when the gas pressure is increased.

This phenomenon is observed in a pressure range of about 0.01 mT to about 12 mT. As with the focused electron beam, the type of gas is not critical. There are differences that can be seen in Fig. 31. However the most important difference is the maximum pressure that the system will operate at before gas breakdown and runaway ionization occurs.

The experimental set-up is shown in Fig. 20 and diagramed schematically in Fig. 32. The ZnS screen in Fig. 20 was replaced with a fully depleted 100 μm surface barrier detector located behind a 0.1 mm slit that was used to reduce the count rate. We used the $LiNbO_3$ crystal described above and shown in Fig. 20. The crystal/heater assembly, which could be moved alone the z-axis of the crystal was mounted axially in a glass cylinder 45 cm long and 7.5 cm in diameter. The glass cylinder was capped by metal end plates. The pressures that we quote here for specific phenomena are unique to the geometry of our set-up. In a different geometry the phenomena we describe will most likely be observed in slightly different pressure ranges. The geometry effect is a question yet to be addressed.

For this study the crystal was heated to about 180 ^{o}C then let cool naturally by turning the heater off when the temperature reached 180 ^{o}C. The data was collected as follows: A pressure is selected, after the pressure stabilized the crystal was cycled from 20 ^{o}C to 180 ^{o}C to 20 ^{o}C. During cooling a 10 sec snapshot of the electron spectrum was collected about every 60 seconds. From these spectra the maximum electron energy for that pressure was determined. These data was then used to construct Fig. 31.

The key to gas amplification is a delicate balance between the rate of polarization charge production (how fast o**r** slow the temperature of the crystal is changing) and the rate at which charge is compensated for with opposite charge from the environment around the crystal. In a low pressure environment (~10^{-6} Torr) polarization charge production will be completed in less than 30 minutes (the temperature is stable at room temperature), however, charge compensation will not be completed for 15 days or more and there will be little if any apparent evidences of gas amplification see trace (a) in Fig. 33. On the other hand, if the pressure is in the 2 mT to 3 mT range, polarization charge production and charge compensation will be completed in less than 30 minutes and the maximum electron energy will be more than twice that observed when the pressure was <10^{-6} Torr as is shown in Fig. 33 trace (b). In both cases polarization charge production

will be completed in less than 30 minutes. In other words the crystal will have cooled to a stable temperature. Figure 34 shows the results when a crystal is thermal in a vacuum of $<10^{-6}$ Torr and not disturbed for 15 days. In Fig 34 we start collecting electron energy spectra on the fifth day after thermal cycling the crystal. After collecting the energy spectrum on the fifteen day we raised the pressure in the chamber to $\sim 10^{-2}$ Torr then returned it to $<10^{-6}$ Torr. The purpose of the pressure change was to compensate or neutralize the remaining polarization charges thereby terminating electron acceleration away from the crystal. A spectrum collected just after the pressure change confirmed that electron acceleration away from the crystal was terminated as is shown by the zero energy point on day fifteen. In Fig. 35 we show electron spectra collected on day fifteen just prior to and after the pressure cycling.

Although the phenomenon of gas amplification is not fully understood we believe the process is as follows: In the pressure range of 3 mTorr during the cooling part of a thermal cycle when by chance a neutral gas molecule approaches close enough to the surface of the crystal it will be ionized. The positive ion will be attracted towards, and ultimately attach to the surface of the crystal thereby compensating for one negative polarization charge. Immediately after ionization but before attachment the electron cloud around the ion will be distorted in the direction opposite to the electric field of the crystal. A dipole is thus formed and is in the process of becoming attached to the negative charge at the surface of the crystal. The electric field of the crystal determines the dipole moment of the just formed dipole. At the start of this process or at pressures $< 10^{-6}$ Torr the strength of the electric field is determined only by polarization charge as is shown in Fig. 33 trace (a) when the temperature was about 100 ^{o}C and electron energies are ~50 keV. Assuming that one electron was removed from the neutral gas molecule, the positive end of the dipole will compensate for just one of the increasing number of negative polarization charges that are being produced as the crystal continue to cool. Once the dipole is attached to the crystal its negative end effective adds negative charge to the surface of the crystal. When the pressure is high (>~0.5 mTorr) there is build up or stacking of dipoles near the surface of the crystal, they are aligned with the crystal E field thus forming plasma extending from the surface of the crystal. We will discuss plasma later. Now the E field is the sum of the remanding uncompensated polarization charge plus the dipole's negative charge. This process continues until the rate of polarization charge production equals the rate of charge compensation. The charge compensation rate is determined by the pressure and is constant at constant pressure and is unique for that pressure. At this point the electric field is at its maximum strength, this is shown in Fig. 33 trace (b) where the maximum electron energy is attained as the crystal cools through ~35 ^{o}C. From this point on the electric field begins decreasing as positive ions (dipoles) continue to compensate the remaining polarization charge. And the dipole moment of the dipoles at and near the surface of the crystal begins to decrease because the field that maintains them is decreasing. In other words the net polarization charge is decreasing, consequently the electric field that distorted the electron cloud around the positive ions to produce the dipoles in the first place is decreasing. Finally when the last polarization charge is compensated for the electric field falls to zero. And the electron clouds around the molecule that are still attached (and will remained attached as long as the crystal is

below the Curie point) to the crystal are no longer distorted. This is the state that the crystal was in when we began the thermal cycle.

Gas amplification is not observed when positive ions are accelerated away from the +z base of the crystal. Evidence of this can be seen in Fig. 36. We see gas amplification of electron energy because, the plasma that forms when the –z base end is exposed does not form when the +z base end is exposed under the exact same conditions. A plasma begins to form at the start of cooling at the –z base because; the increasing negative charge in the surface of the crystal results in the production and attraction, of molecular dipoles, simultaneously the attending clouds of electrons around the dipoles are further distorted as the dipoles approaches the negatively charged surface of the crystal. On the other hand when molecules are ionized at the +z base, electrons are attracted to the increasingly positively charged surface of the crystal and the positive ions with their attending clouds of electrons are accelerated away, hence no plasma formation at the +z base during cooling and we therefore do not get gas amplification of positive ions. In terms of a unit charge, when an electron compensates a positive polarization charge the net electric field strength is reduced by an amount equivalent to exactly one unit of charge. Whereas in the case of the -z surface when a positive ion compensates for one negative charge we have the distorted cloud of electrons left over after the polarization charge has been compensated for. The electric field strength is in fact now increased above what was produced by the polarization charge alone because of the presence of this electron cloud. At the +z base the electric field is produced only by polarization charge. In Fig. 37 and 38 we show the relationship between electron energy and the very loosely held negative charge (plasma) at the surface of the –z base of a crystal. We show in Fig. 37 how a smooth reduction in pressure over about 25 seconds will cause a sudden increase in electron count rate at the start of pressure change. This is caused by expulsion of the plasma from around the surface of the crystal due to the pressure change. Immediately after expulsion the electron count rate drop to well below what it was before the pressure changed. This is consistent with the idea that the electric field strength has been reduced and therefore fewer molecules are now being ionized to free electrons to be counted. In Fig. 38 we show three electron spectra, (a) was collected just before the start of pressure change, here the electron energy was 138 keV. In (b) we show a spectrum collected immediately before and during the 1st 20 seconds of the pressure changing. Here we see two peaks P1 and P2, P2 appears simultaneously with the start of pressure change this indicating an abrupt change in electron energy. In (c) we show an electron spectrum collected at the new lower pressure. The electron energy is about what it would have been if the crystal had been thermally cycled at a pressure below about 10^{-6} Torr.

The electric field strength at the end of expulsion is due only to the negative polarization charge. The plasma may be removed by several methods and the effect is the same. For example, a sudden movement of the crystal or if the crystal is rotating and the angular velocity is increase above a threshold the plasma will be dislodged and the electric field strength will be reduced.

Photon Fluoresced X-Ray Spectra

The main object of this work is to show that nearly background-free bremsstrahlung fluoresced K x-rays of elements up to Pb (Z = 82) can be produced by pyroelectric crystal electron accelerators if the process of ”gas amplification", which has been described above and in ref 12 for electrons is taken advantage of. A secondary object is to show that gas amplification occurs on cooling but not on heating for a given crystal by means of the x-ray spectra. The idea is that optimizing the ambient gas pressure can more than double the maximum electron energy. When the -z base of a pyroelectric crystal is exposed to dilute gas during cooling, gas molecules in the vicinity of the crystal are ionized[7] and plasma is formed near the negatively charged surface. The resulting positive ions are attracted to the crystal surface thus reducing its negative charge as well as the electron energy while; the electrons are focused by the plasma and accelerated away from the crystal.[12,28,29] The maximum energy of electrons produced during cooling can be varied by a factor of more than two by varying the gas pressure surrounding the crystal between 0.1 mTorr and about 10 mTorr.[20] On heating a crystal when its surface is positive the gas amplification effect is inoperative. This is demonstrated via the observed x-ray spectra where the bremsstrahlung end-point energy is about half of what it is on cooling as explained below.

When the +z base of a crystal is exposed to dilute gas during cooling positive ions are focused and accelerated away from the crystal while electrons are accelerated toward and impinge on the crystal producing x rays and bremsstrahlung at the surface of the crystal[12]. We used these crystal x-rays and bremsstrahlung to produce relatively background-free fluoresced K x-rays of lower Z elements The Si(Li) X-ray detector was in the target chamber vacuum. No spectra from this set up are shown since no high-energy electrons were produced by the gas amplification mechanism.

Except for the commercially produced pyroelectric crystal x-ray generator by Amptek[4] whose maximum bremsstrahlung energy is about 35 keV, no studies of the behavior of these crystals in dilute gases, for the production of high-Z K x ray production, have previously been reported. An experimental arrangement which produces the highest energy radiation, is shown schematically in Fig. 39 where a 4 mm dia x 10 mm $LiNbO_3$ crystal with its –z base exposed produces a focused electron beam[28,29] which impinges on a composite target of W/Bi. This gives rise to high-energy bremsstrahlung and W/Bi K x-rays, which were used to fluoresce K X-rays of Ta and Pb. The bremsstrahlung and W and Bi K X-ray fluoresced spectrum of a metal foil of Ta is shown in Fig. 40(a) The K x-ray spectrum is very free of background because the cross section for K-shell ionization by photons whose energy is just above the Ta K-shell ionization energy is much greater than the cross section for Compton and elastic scattering of the lower and higher energy bremsstrahlung by the Ta target. Figure 40(b) shows the spectrum obtained when electrons rather than photons directly bombard the Ta target. The peak-to-background ratio is much smaller. The Ta L x-ray spectrum is very prominent too but the peak-to-background ratio is not as good as for the K x-rays. The peak to background ratio for this spectrum is more than a factor of two better than the Ta

K X-ray spectrum obtained with 5.6 MeV gamma rays at the Duke Free Electron Laser (FEL).[30]

Bremsstrahlung fluoresced Sn K x-rays superimposed on attenuated Bremsstrahlung spectrum arising from electron bombardment of Pt is shown in a linear display in Fig. 41(a). The geometry is collinear as shown above in the inset. The log display of the Pt/Sn spectrum in Fig. 41(b) is multiplied by an arbitrary number for display purposes. The electron-excited Pt L x-rays, which are attenuated by the Sn are prominent. The crystal was $LiNbO_3$ (5mm long) with its -z base exposed and the Nb K x-ray spectrum, which was produced during heating to 160 ^oC, is shown as well as the asymmetry of gas amplification. The Pt/Sn target was removed during heating for this run to permit observation of Nb L x-rays. The Pt/Sn target removal had minimum effect on the end point energy. We have observed gas amplification only on cooling when the –z base is exposed, the bremsstrahlung end point energy in this case is about 65 keV while in the heating mode, at the same pressure, the bremsstrahlung end point energy is about 33 keV. While the end point energy will change with pressure on cooling, during heating the end point energy is virtually unchanged. This suggests that there is no plasma energy-enhancing process occurring when the crystal surface is positive, while when the crystal surface is negative a plasma energy-enhancing effect occurs. When the crystal's surface is negative and the crystal is cooling i.e., the –z base is exposed, the plasma at the surface of the crystal may be displaced in several ways. A gradual or sudden change in the gas pressure causes the plasma to be expelled from the crystal. This is illustrated in reference 20, Figs. 2 and 3, reference 7 in Figs. 6, 7 and 9 and reference 31. The plasma may also be separated from the crystal by a sudden violent movement of the crystal from a stationary position or by increasing the angular velocity when the crystal is rotating in dilute gas.

Figure 42 shows the x-ray spectrum of bremsstrahlung fluoresced Pb combined with leak-through Bi K x-rays from the W/Bi target. The count rate was very low here so two thermal cycles were required and the detector could view a little bit of the target, the source of the Bi. Nevertheless this proves that the electron energy was > 90.5 keV, the Bi K-shell ionization energy.

In conclusion we show how heated and cooled cylindrical pyroelectric crystals such as $LiNbO_3$ and $LiTaO_3$ under the right conditions can be used to produce relatively background-free characteristic K x-ray spectra for high-Z elements. We compare these spectra with electron-excited spectra, where the background is much larger, and we show how the gas amplification process can be observed via x-rays when the crystal surface is negative whereas no electron-energy enhancement occurs when the crystal surface is positive.

Using Crystal X-Ray Generators

The crystal electron accelerator is an excellent low cost tool to use in study the elemental uptake in tree leaves and other growing plants. With this tool it is easy to distinguish between the top and under side of leaves through the growing season and therefore follow the uptake and location of elements in leaves across the growing season.

The tools needed are shown in Fig. 47. They are a low energy X-ray detector and data acquisition system, small vacuum chamber with a vacuum pump. A crystal of $LiNbO_3$ or $LiTaO_3$ that is about 1mm thick and 5mm X 5mm will not accelerate electrons to an energy high enough to penetrate leaves when they first unfold in the spring. Therefore, by irritating first one side then the other one can determine which elements are present and their relative concentration. The element cutoff is determined by the thickness of your x-ray detector window thickness therefore low Z element (Z< about 12) may not be detected.

The pignut hickory (*Carya glabra*) is perhaps, one of the more spectacular examples of polar concentration and timing of element uptake in trees. X-ray spectra data is presented in Fig. 44 shows the element content in the surface of leaves collected from first unfolding in early spring through leaf dropping in the fall. The first set leaves were on May 20, when they were less than three days old. Notice that there is little distinction in element content on the topside and underside of the leaves at this early stage in leaf development. However, as the leaves grow and mature a clear distinction developed between the topside and underside.

In pignut hickory the accumulation of Mn began between May 20 and May 31, Ca, May 31 and June 13, and Al, June 24 and July 1. The pignut hickory is not unique in showing this kind of uptake pattern, however, it does appear to be unique with respect to Al and Mn uptake and location in the leaf.

When the leaves of all the trees in this study first unfold they look very similar to the newly unfolded pignut hickory, however, within days they began to "take up" elements in a paten that appear to be unique to each species and sometime unique to a specific tree within a species even when branches and roots overlaps.

In this study leaves were collected from the same trees at regular interval (7-10 days) from the date of first appearance until leaf drop in the fall. Usually, five leaves were collected and immediately dried. We vacuum dried most of the leaves used in this study, however oven drying work equally as well. To analysis the leaves a small sample of each leaf (about 2 cm^2) is placed in X-ray fluorescence spectrometer shown in Fig. 43 and X-ray spectra of elements in the leaf surface were produced by cycling the crystal through one temperature cycle. The leaf sample is then rotated 180^o and the procedure is repeated. This is key to the determination of element content in top and under sides of leaves to a depth of less than 2μm. Information about the interior the leaf was obtained by pulverizing the sample and analyzes the powder, the usual method.[33] Figure 45 is a typical example of the type of information that is both lost and gained when a leaf is pulverized. It is clear that the Ca/Al and the Ca/Mn ratios are dramatically different for each analysis. All three analyses were done on the same leaf sample and normalized to the same count in a region of the spectra around 3 keV. When this was done, the relative concentration of each element in the leaf is inferred from number of counts in each peak. It is clear that most of the Al is in the topside layer and vertically all of the Mn is in the underside layer of the leaf. Potassium, S and Cl are mostly concentrated inside the leaf. This information is totally lost when traditional methods are used.

Conclusions

We have described many new phenomena that can be observed when a crystal of $LiNbO_3$ or $LiTaO_3$ is heated and cooled in a dilute gas. They are: (1) A self-focusing electron beam going away from the crystal. (2) A self-focusing electron beam coming towards the crystal. (3) A self-focusing positive ion beam going away from the crystal. (4) We believe that there is a self-focusing positive ion beam going towards the crystal although we have not observed it. (5) The source of the electrons and positive ions is field ionization via tunneling in the residual gas molecules that surround the crystal. (6) The energy of the electrons in the beam can be increased by optimizing the pressure of the gas in the chamber that houses the crystal. (7) There is no corresponding increase in positive ion energy when the pressure of the gas is increased. (8) Electrons accelerated away from the vicinity of the crystal are nearly monoenergetic. (9) A crystal will continue to accelerate electrons nearly monoenergeticly for more then 15 days following a heating cycle. (10) The self-focused beam will remain stable for more than 16 hours. (11) The production of characteristics x rays of elements with a Z as high as Bi. (12) How to build a crystal X-Ray Generator without grounding the crystal or the target. Many of these phenomena have not been described before or were miss interpreted.

There are many future possibilities for further study and development. For example there has been no systematic study of the rate of heating and cooling on the intensity and energy of electron and ion beams. The main crystals, which we have studied so far, are $LiNbO_3$ and $LiTaO_3$ but there are many more pyroelectric crystals, which have not been studied from the point of view of producing electron and ion beams. There are numerous opportunities to study the spectral and other characteristics of the plasma generated in the gas under the changing high electric field conditions. There is a broad field of study of the effects of crystal size and shape on the electron and ion beams. Further more the geometry and material of the chamber, which houses the crystal, needs thorough study. So far almost no mathematical modeling has been done of the phenomena described here.

There are many possibilities of practical applications for example by taking advantage of gas multiplication it should be possible to commercially developing a portable high energy x-ray source for x-ray fluorescence of rocks, tree leaves high-Z nuclear bomb materials etc. One idea which we have not yet been able to pursue is to develop a neutron source by surrounding a pyroelectric crystal with deuterium gas and using the 110 keV D+ ion beam to bombard a tritium target so as to produce 14 MeV neutrons.

We are most grateful to our colleagues, Sol Raboy, Eugene Merzbacher, Tom Clegg and Bill Hooke for many insightful discussions and continued encouragement.

References

1. S. B. Lang, Sourcebook of Pyroelectricity, Gordon and Breach, New York (1974).

2. Peter Fritz Bräunlich, United Stated Patent No**. 3,840,748** (1974)

3. James D. Brownridge, Nature, **358**, 287, (1992)

4. Amptek Inc., 6 De Angelo Dr., Bedford, MA 01730, www.amptek.com

5. G. Rosenman, D. Shur, Ya. E. Krasik and A. Dunaevsky, J. Appl. Phys. **88**, 109 (2000).

6. J. F. Nye, Physical Properties of Crystals, Clarendon Press, Oxford (1957)

7. James D. Brownridge and Sol Raboy, J. Appl. Phys., **86**, 640 (1999)

8. D. Shur, G. Rosenman, and Ya. E. Krasik, Appl. Phys. Lett. **70**, 574 (1997).

9. Weiming Zhang, Wayne Huebner, Stephen E. Sampayan and Mike L. Krogh, J. Appl. Phys. **83,** 6055 (1998).

10. S. M. Shafroth , W. Kruger and J.D. Brownridge, Nucl. Instr. and Meth., **A 422**, 1 (1999)

11. S. M. Shafroth and J. D. Brownridge, CP 475 American Institute of Physics , Applications of Accelerators in Research and Industry, Edited by J. L. Duggan and I. L. Morgan, p 1100 (1999)

12. J. D. Brownridge, S. M. Shafroth, D. Trott, B. Stoner, W. Hooke, Appl. Phys. Lett, **78**, 1158 (2001)

13. B. Rosenblum, P. Braunlich and J. P. Carrico, Appl. Phys. Lett. 25, **17** (1974)

14. James D. Brownridge and Sol Raboy, Preprint at **http://arxiv.org/ftp/physics/papers/0107/0107046.pdf**

15. J. D. Brownridge and S. M. Shafroth, Appl. Phys. Lett., **79**, 3364 (2001)

16. V. D. Kuget, G. Rosenman and D. Shur, J. Phys. D: Appl. Phys., **28**, 2360 (1995)

17. E. V. Minakova, N. A. Tikhomirova and Yu. A. Khrustalev, Phys. Chem. Mech. Surfaces, **5**(7), 1861 (1990)

18. V. S. Kortov K. K. Shvarts, A. F. Zatsepin, A. I. Gaprindashvili, A. V. Guilbis and Z. A. Grant, Sov. Phys. Solid State **21**(6), 1093 (1979)

19. S. P. Gribkov, V. S. Zal'tsberg, V. I, Nosova and V. E. Risin, Sov. Phys. Solid State **33**(1**)**, 368 (1991)

20. James D. Brownridge and Stephen M. Shafroth, Appl. Phys. Lett., **83**, 1477 (2003)

21. James D. Brownridge and Sol Raboy, Preprint at **http://www.arxiv.org/ftp/cond-mat/papers/0205/0205189.pdf**

22 S. C. Abrahams, E. Buehler, W. C. Hamilton and S. J. Laplaca, J. Phys. Chem. Solids, **34**, 521 (1973)

23. Sungwon Kim, Venkatraman Gopalan, K. Kitamura and Y. Furukawa, J. Appl. Phys. **96**, 2949 (2001)

24. G. Rosenman, Ferroelectric, **126**, 305 (1992)

25. G. Rosenman and I. Rez, J. Appl. Phys., **73**, 1904 (1993)

26. R. S. Weis and T. K. Gaylord, Appl. Phys., **37**, 191 (1985)

27. J. Kalinowski and Z. Dreger, Phys. Rev. B., **36**, 7840 (1987)

28. J. D. Brownridge and S. M. Shafroth, Int. Nat. Conf. On High Power Electron Beam Technology, Hilton Head, S.C. (2002) and http://www.arxiv.org/ftp/physics/papers/0209/0209079.pdf

29. J. D. Brownridge, Video clip, Dynamical Behavior of Beam as Pressure Increases, http://www.binghamton.edu/physics/brownridge.html

30. Private communication, H. Weller and TUNL Progress Report 2002-2003 and Phys. Rev. Lett. **88**, 012502 (2002).

31. H. Riege, Appl. Surface Sci.,**111,** 318 (1997)

32 G. I. Roseman, V. I. Pechorskii. Yu. L. Chepelev, E. I. Boikovc and L. E. Issakova, Phys. Stat. Sol., (b) **120**, 667 (1983)

33. V. Kocman, T. E. Peel and G. H. Tomlinson, Commun. Soil Sci. Plant Anal. **22**, 2063 (1991).

34 V. I. Nagaychenko, V. M. Sanin, A. M. Yegorov, A. V. Shchagin. Preprint, 2003 at http://www.arxiv.org/ftp/physics/papers/0309/0309049.pdf

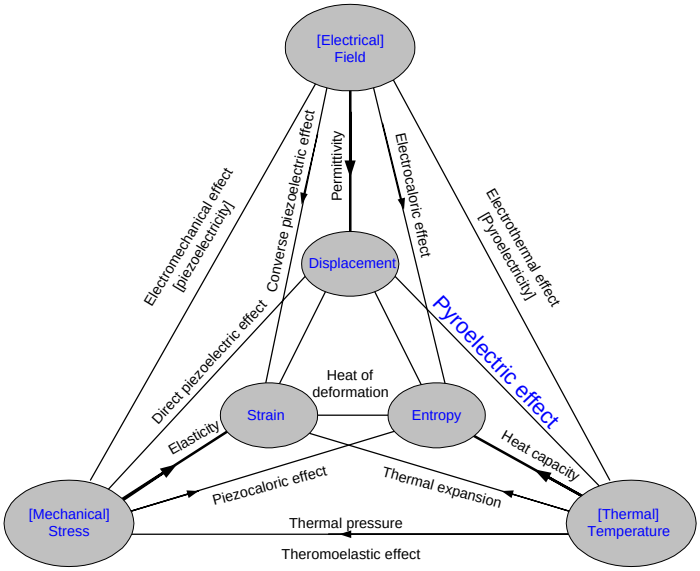

Fig. 1 Relationship between electric field, temperature and mechanical stress.

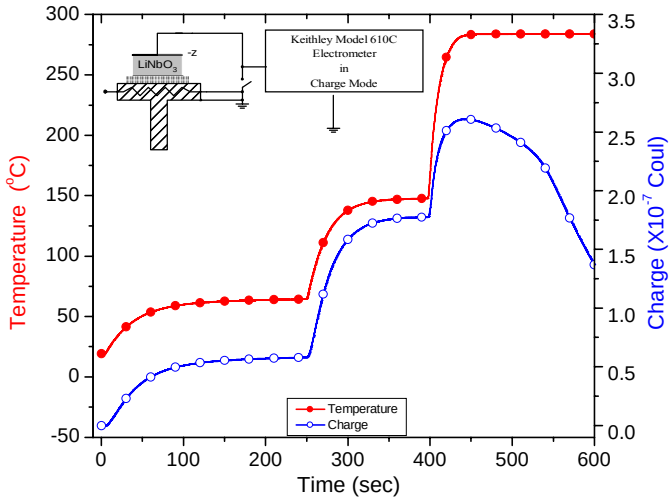

Fig. 2 With metal electrodes on the +z and the -z base of a 4 mm diameter by 10 mm long $LiNbO_3$ crystal and the +z not grounded, charge was measured at the -z base as the temperature was raised. The experimental set-up was as shown in the insert.

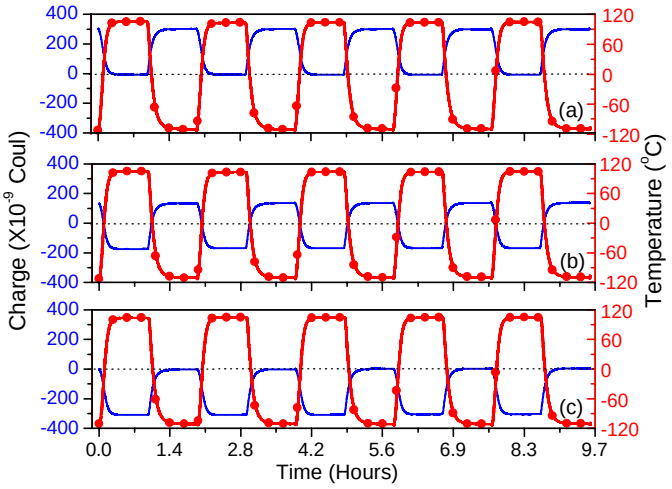

Fig. 3 Polarization charge and temperature as functions of time for the +z base of a crystal of $LiNbO_3$, with a thickness of 1.000±0.001 mm and a base 5.351±0,003 mm by 3.811±0 001 mm. In all three zeroing conditions presented the curve with solid circles represents the temperature. The solid curve represents the relative charge reading of the electrometer. (a). The electrometer was grounded at a crystal temperature of 100°C. (b). The electrometer was grounded at a crystal temperature of 0°C. (c). The electrometer was grounded at a crystal temperature of -110°C.

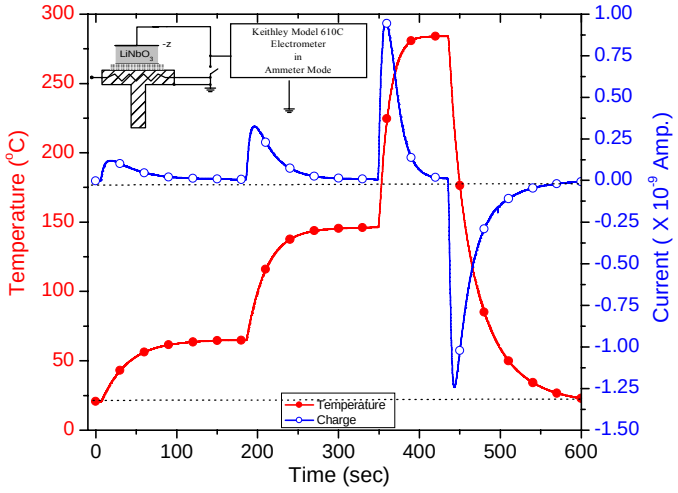

Fig. 4 With metal electrodes on the +z and the -z base of a 4 mm diameter by 10 mm long $LiNbO_3$ crystal and the +z grounded, current was measured at the -z base as the temperature was raised in three steps to ~285 ^{o}C. The experimental set-up was as shown in the insert.

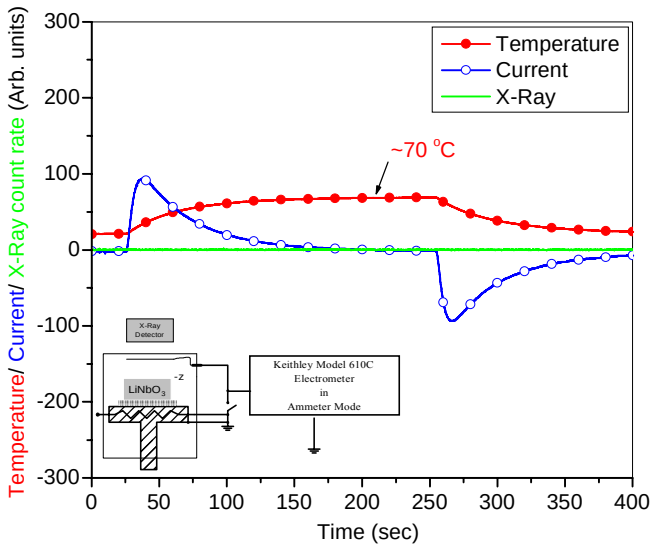

Fig. 5 The electrometer probe is separated from the crystal by 1cm and also serves as the target for electrons accelerated away from the crystal on cooling. If the electrons are energetic enough they will excite atoms in the target producing x rays. In this case they are not. During warming electrons are accelerated to the crystal exciting atoms in the crystal and producing x rays if they are energetic enough. In this case they are not.

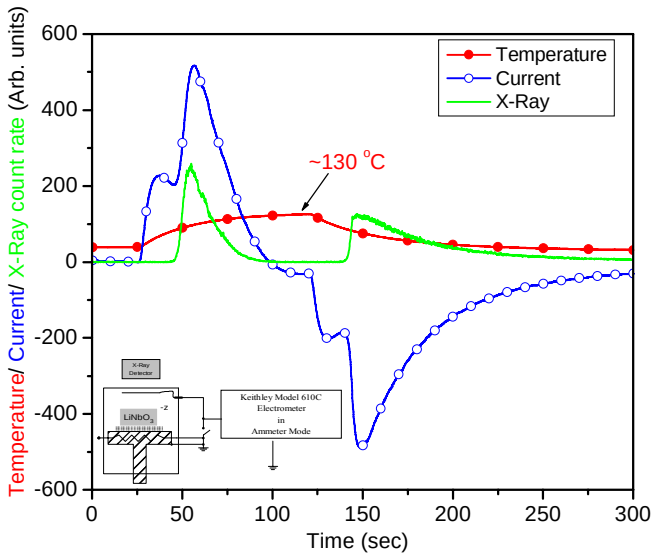

Fig. 6 The electrometer probe is separated from the crystal by 1cm and also serves as the target for electrons accelerated away from the crystal on cooling. In this case the electron are energetic enough to excite atoms in both crystal and the target thereby producing x rays that we detect with the x-ray detector. The onset of x ray production can also be inferred from a change in direction and the absolute magnitude of the current. During warming electrons are accelerated to the crystal and on cooling they are accelerated away.

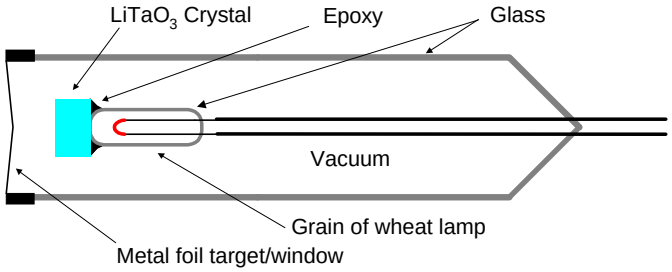

Fig. 7 Shows an all glass model of a crystal x-ray generator that demonstrated that no part of the crystal/target system needed to be electrically grounded. The glass tube is ~8 cm long and ~1 cm in diameter.

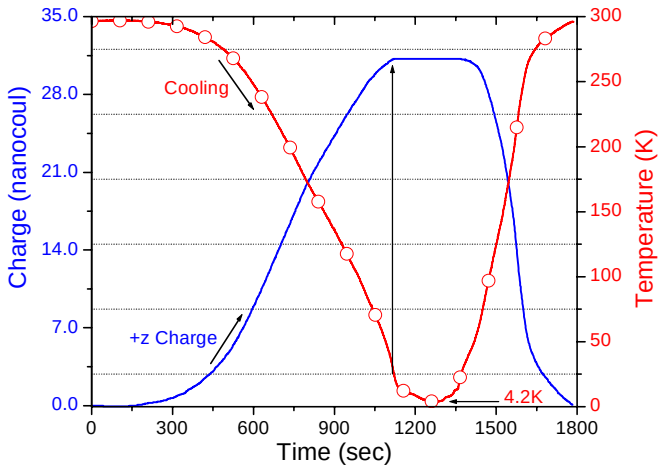

Fig. 8. A $LiNbO_3$ crystal is subjected to a temperature change of 300K to 4.2K and back to 300K in one continuous cycle. The line with open circles is the temperature and the solid line is the spontaneous polarization charge on the +z base of the crystal. The base area of the crystal was 10.19±0.04mm^2 and its thickness was 1.001±0.001mm. The "polarization saturation temperature" for $LiNbO_3$ is 14.09± 0.05K. The temperature below which charge no longer changes with deceasing temperature.

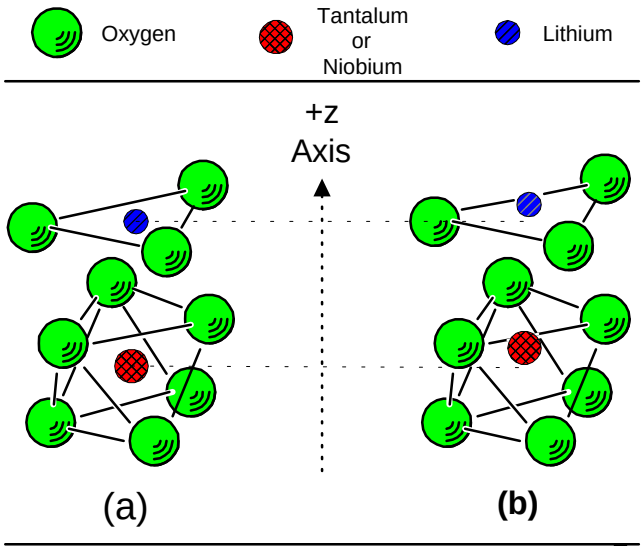

Fig. 9 A schematic diagram of an abbreviated unit cell of $LiNbO_3$ and $LiTaO_3$, their crystallographic structure is quite similar. Here we show the position of the Li and Nb/Ta atoms relative to the plane of oxygen atoms when the crystal is (a) above the Curie temperature and (b) when it is below the Curie temperature. The further below the Curie temperature the further the Li, Nb and Ta atoms move with respect to the oxygen atom planes.

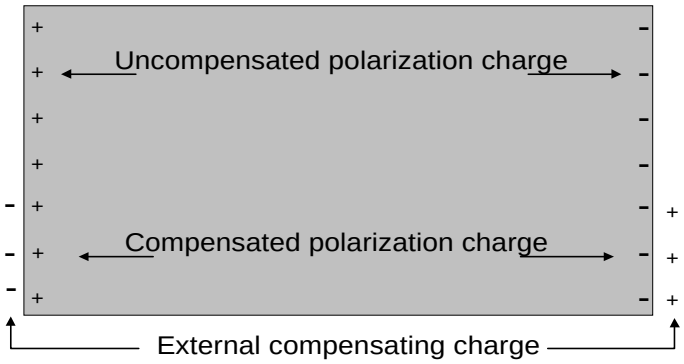

Fig. 10 A schematic diagram of a pyroelectric crystal shortly after a temperature change when the crystal is in a vacuum. The uncompensated polarization charges produce an electrical field external to the crystal.

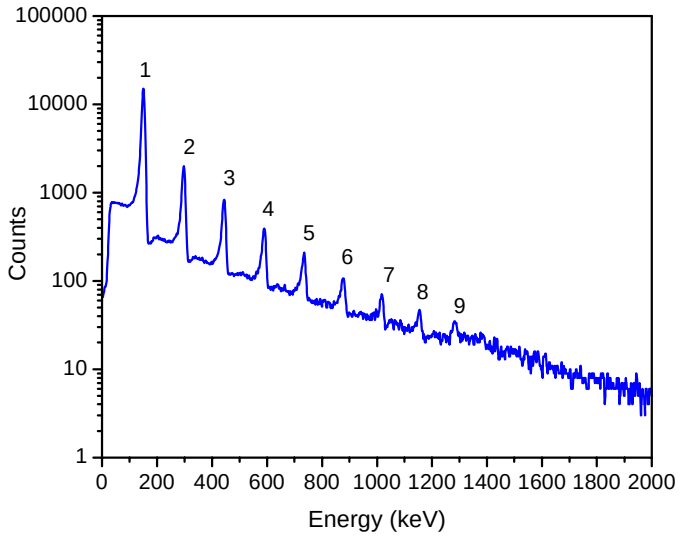

Fig. 11. Shows **a** typical electron spectrum when the crystal is cooling through about 40 ^{o}C. Data was collected for about 10 second**s**. The energy spacing of the peaks is equal to the energy of the first peak and is the result of self-focusing i.e.1, 2, 3 etc. electron**s** arriving at the detector within the resolving time of the electronics. Multiple peaks are seen even when the counting rate is <10 c/s.

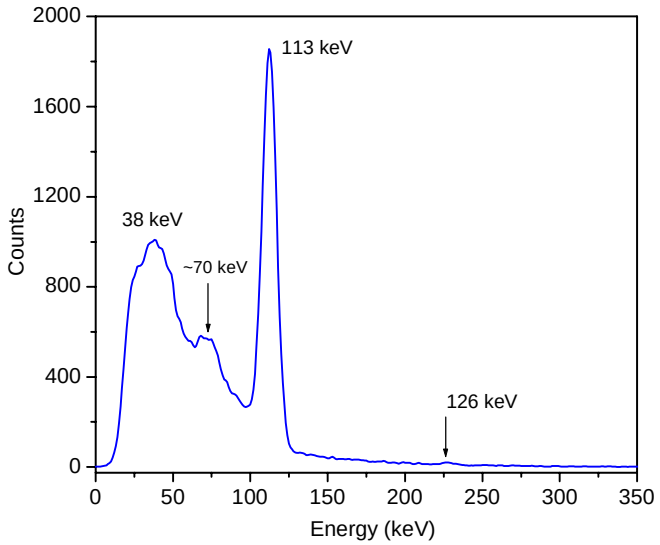

Fig. 12. Shows a positive ion spectrum when CO_2 is the residual gas at 2 mTorr and the crystal temperature **is** passing through 53 ^{o}C **while** cooling. The +z end is exposed.

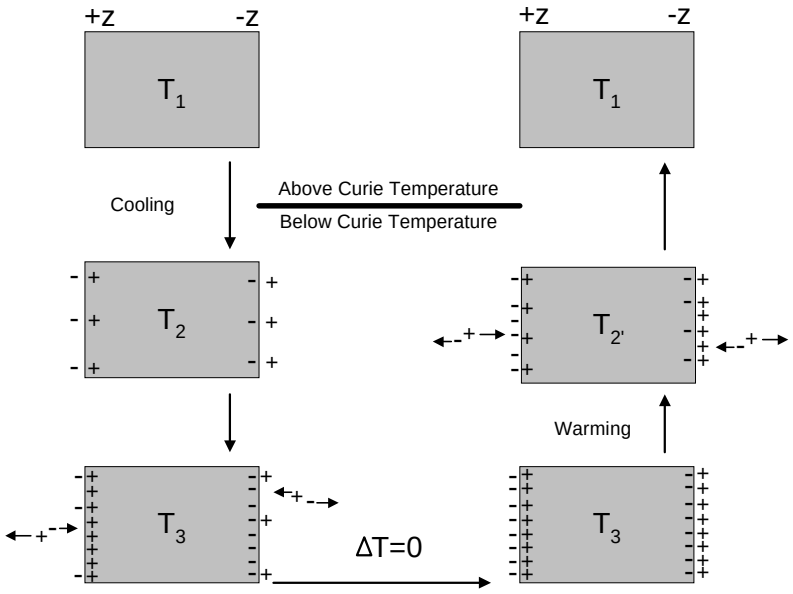

Fig. 13 Schematic diagram to provide a descriptive picture of the response of the environment of the pyroelectric crystal to changes in the polarization charge induced by changes in the temperature of the crystal**. Initially the negative polarization on the right side builds up as the crystal cools The temperature is then held at T3 until all polarization charge is compensated (bottom right). Then as the crystal warms to T2 there is less negative polarization charge on the right side so that positive charge exceeds negative polarization charge and positive ions are repelled while electrons are attracted as indicated.** It is to be noted that this picture does not correspond to any definite pressure of the gas in the vacuum system.

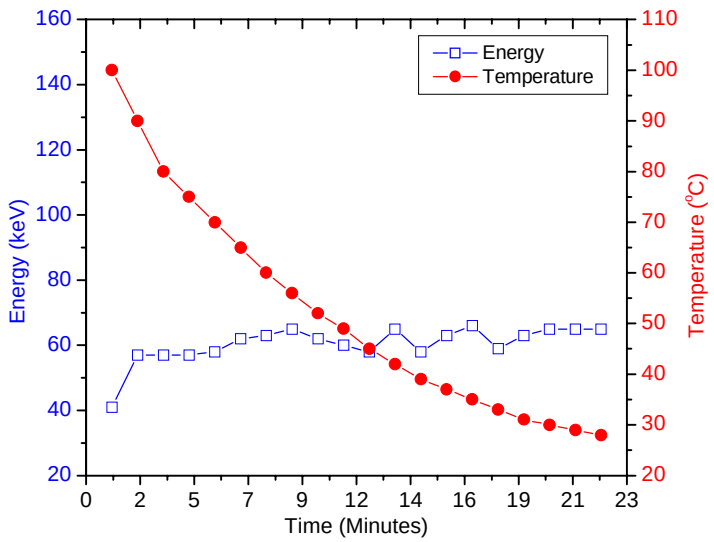

Fig. 14 shows the energy of electrons that are accelerated away from a 4mm diameter by 10 mm long $LiNbO_3$ crystal. Data was collected for 10 seconds at each time interval in order to determine the average electron energy for those 10 seconds. The crystal was cooling from ~100 ^{o}C to ~27 ^{o}C and its temperature is shown for each 10 second interval. The pressure in the vacuum chamber was <8X10^{-7} Torr. **There is little change in electron energy as expected since most of the gas is evacuated i.e. no gas multiplication of the electron energy.**

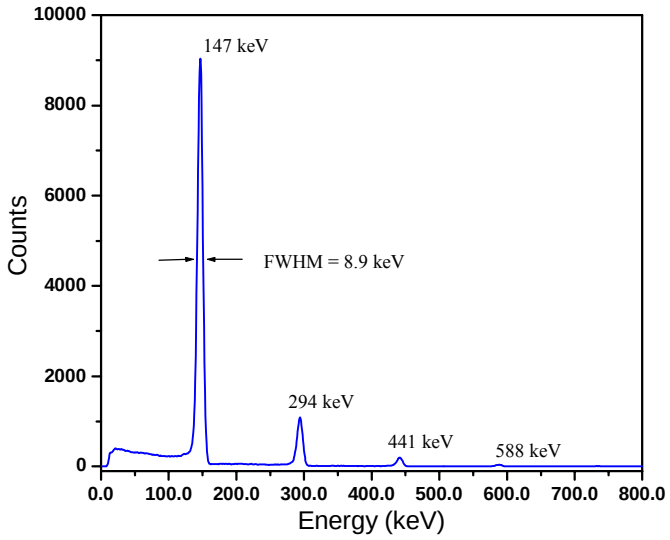

Fig. 15 A typical electron spectrum collected during a 10 second interval as the $LiNbO_3$ cools **to** about 45 ^oC as depicted in the Fig. 13 between T_2 and T_3 and as shown by the data in presented in Fig. 16.

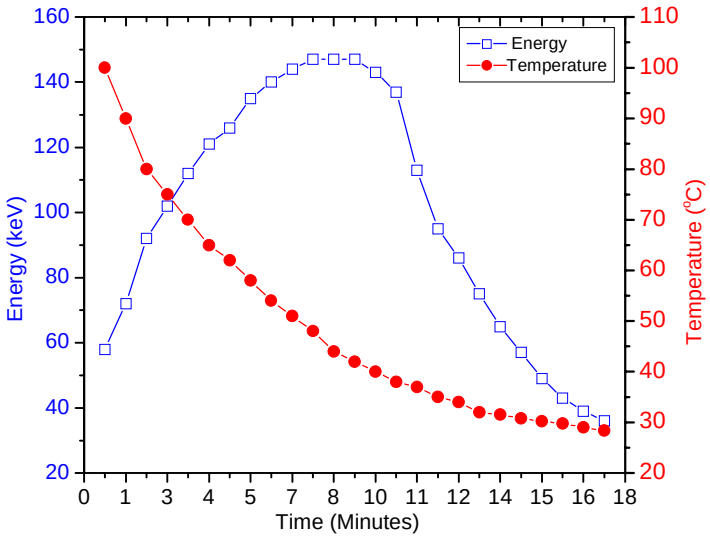

Fig 16 shows the energy of electrons that are accelerated away from a 4mm diameter by 10 mm long $LiNbO_3$ crystal. Data was collected for 10 seconds at each time interval shown in order to determine the average electron energy for those intervals. The crystal was cooling from ~100 ^oC to ~27 ^oC and its temperature is shown for each time interval. The pressure in the vacuum chamber was ~10^{-3} Torr. The dramatic change in energy is due to gas amplification.

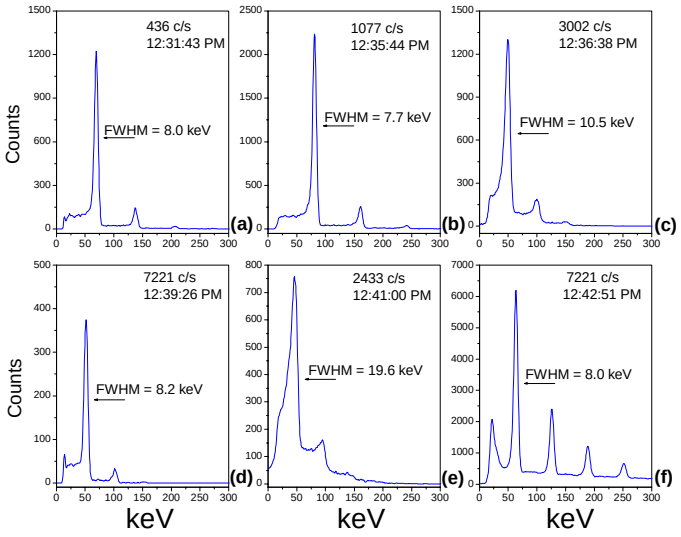

Fig. 17 The multiple electron peaks shown in Figs. 11 and 15 can be distorted by perturbing the plasma at the surface of the crystal. Here the pressure was very gradually varied in the vacuum chamber over time and the shapes of the peaks respond. Notice how the FWHM of the peaks change with time as the pressure changes. The change is clearly not due to a counting rate effect.

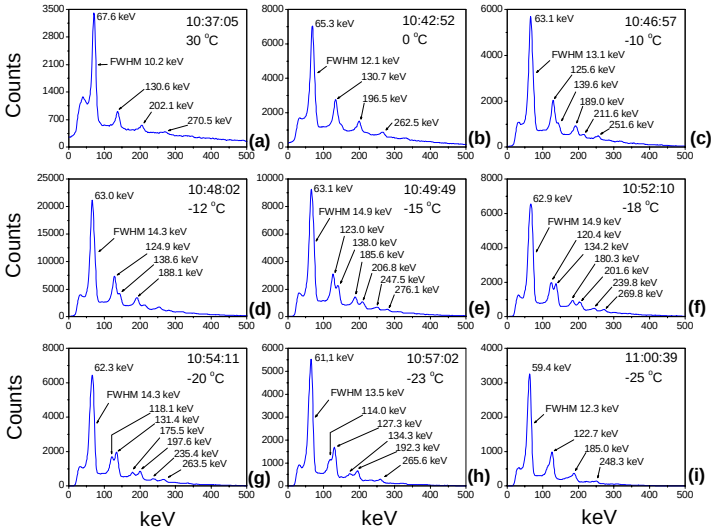

Fig. 18 Shows multiple single electron peaks "splitting" into twin peaks and returning to single peaks during a continuous cool down from 170 ^{o}C to -25 ^{o}C. Data is shown between 30 ^{o}C and -25 ^{o}C where the phenomenon is most dramatic.

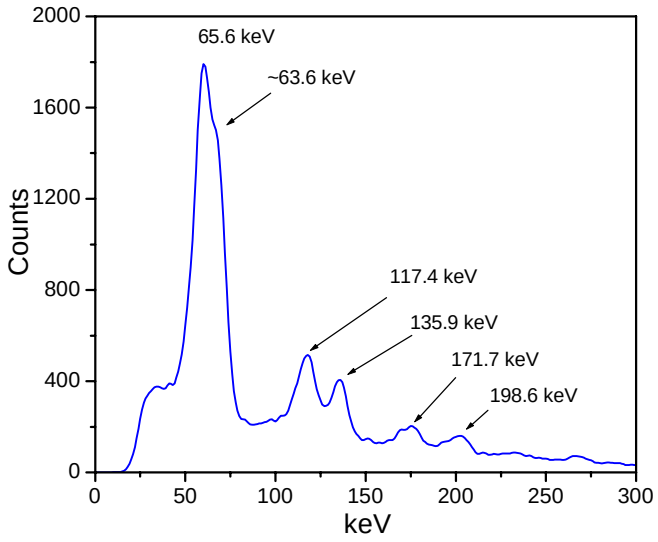

Fig. 19 Shows a spectrum where the "splitting" is clearly evident in every electron peak.

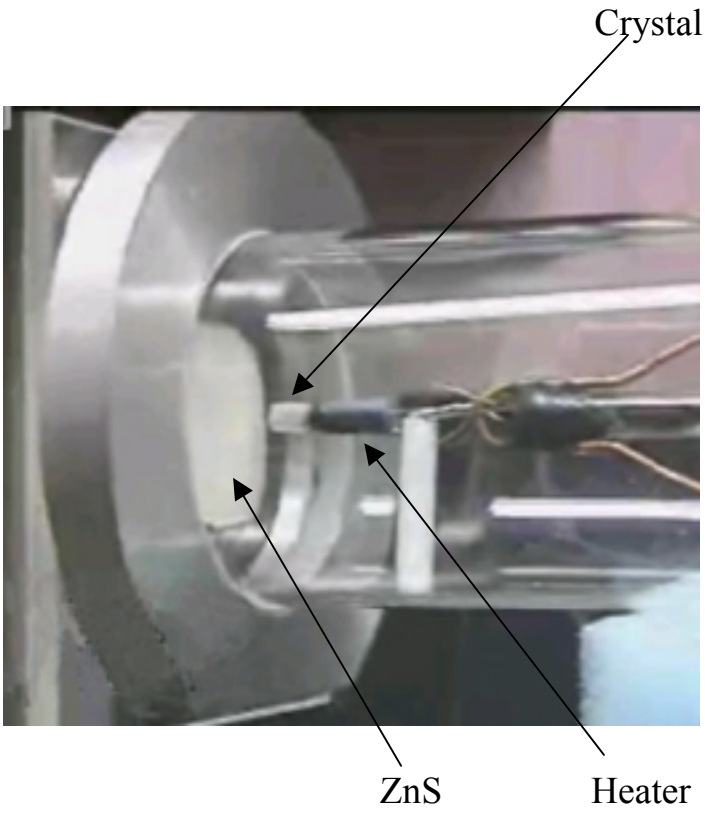

Fig. 20 Photograph of the crystal/heater assembly inside a glass cylinder 45 cm long and 7.5 cm. The ZnS screen is held at the end of the tube by an aluminum ring.

Fig. 21 Photograph of the electron beam image at the focal length, 22mm **for a 4 mm dia x 10 mm long** LiNbO3 crystal. . A ZnS screen was used to image the beam.

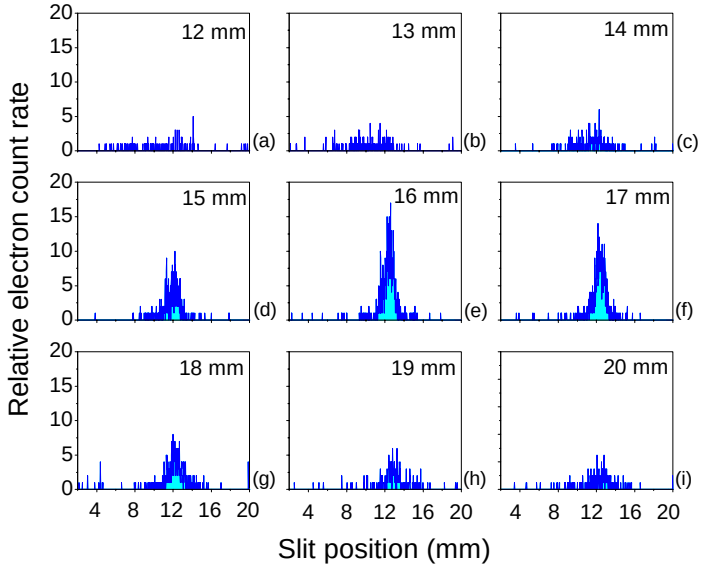

Fig. 22 Results of beam scans at different crystal-to-slit distances 16 hours after the crystal was heated from ~20 ^{o}C to ~115 ^{o}C then allowed to cool back to ~ 20 ^{o}C.

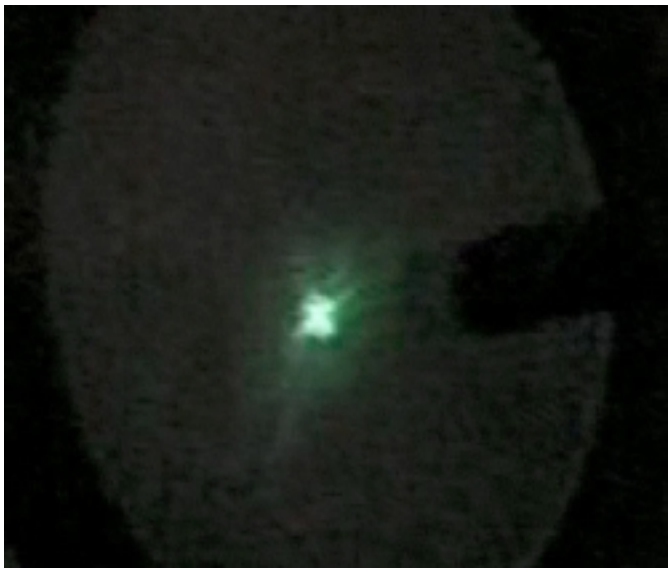

Fig. 23 Photograph of the electron beam image as the pressure rise**s** through about 3mTorr and the beam begin to defocus and become unstable

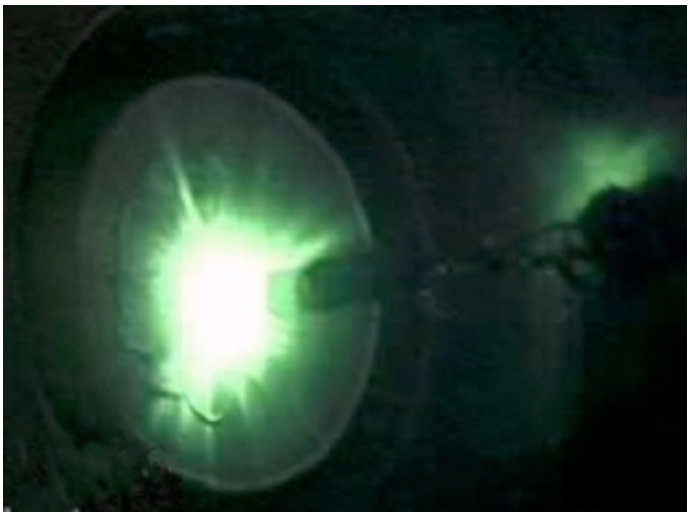

Fig. 24 Photograph of the electron beam image as the pressure rise **to** about 8 mTorr and the beam blow**s** up in runaway ionization of gas around the crystal.

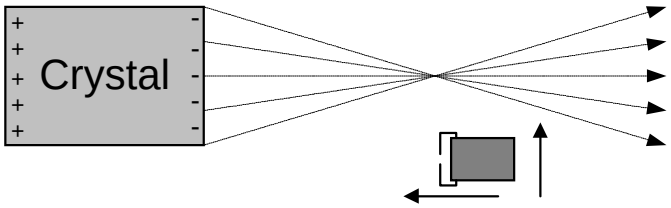

Fig. 25 Idealized cartoon of a crystal focusing an electron beam. Moving an electron detector as indicate by the arrows **allows** beam profiles to be made.

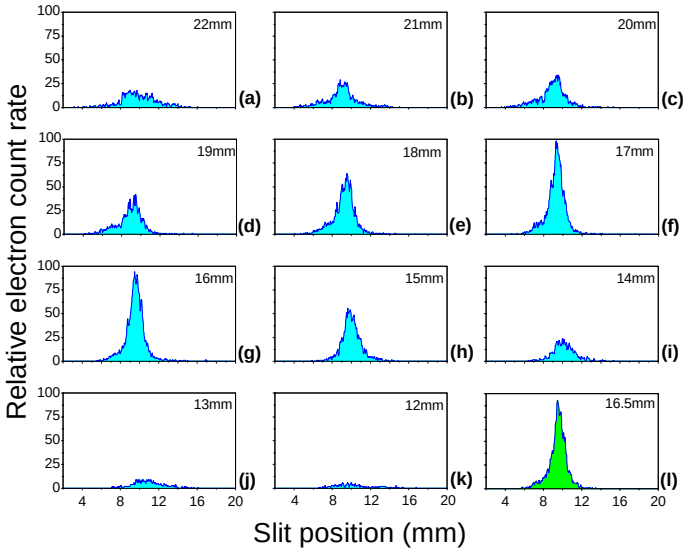

Fig. 26 Results of beam scans at different crystal-to-slit distances about 30 minutes after 5 mm long 10 mm in diameter $LiNbO_3$ crystal was heated from ~20 ^oC to ~115 ^oC then allowed to cool back to ~ 20 ^oC. The scans were made sequentially beginning at 22mm. The focal length is ~17mm.

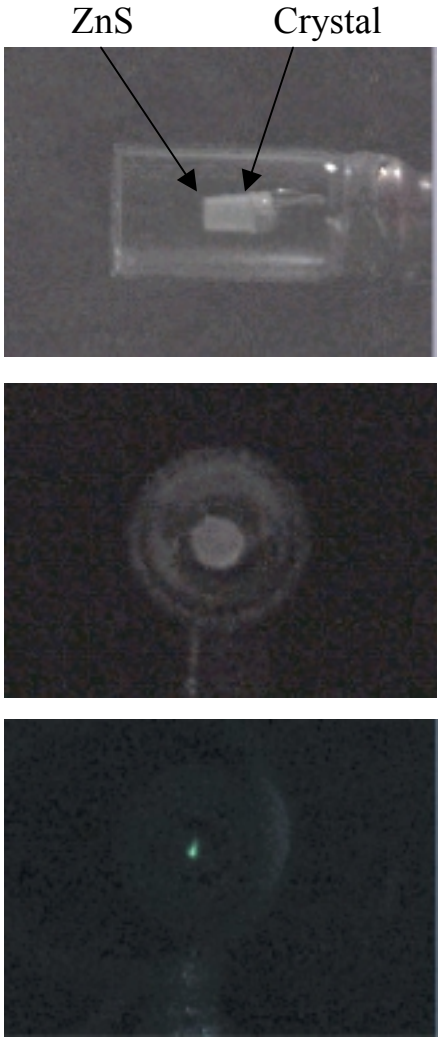

Fig. 27 (a) A 6mm diameter by 10mm long $LiNbO_3$ crystal is shown inside a glass vacuum tube that is 25mm in diameter and 45mm long. (b) Shows the end view of the ZnS covered +z end of the crystal as seen through the glass vacuum tube. The pressure is ~0.1 mTorr, the gas is air. (c) Shows the fluorescent spot where electrons strike the crystal after the beam has self-focused.

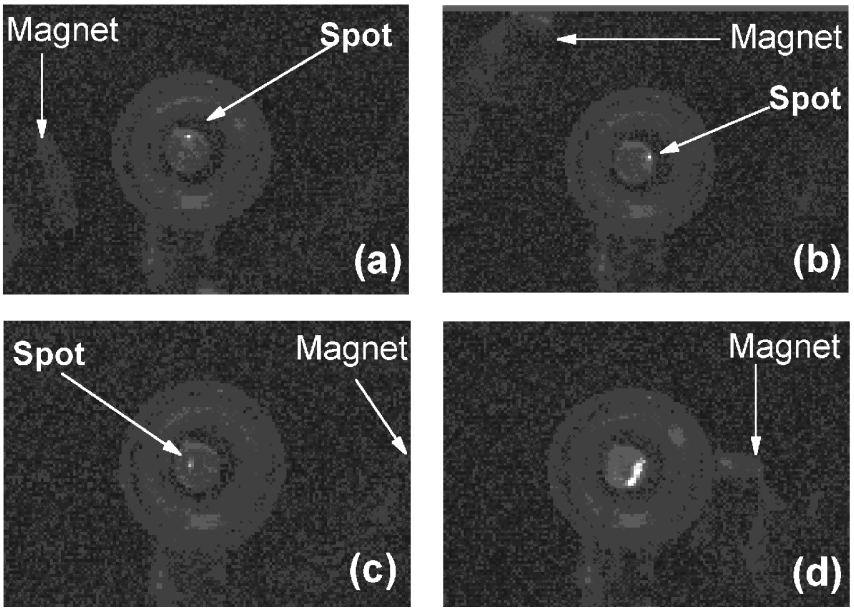

Fig. 28 Shows the electron beam spot location relative to the position of a magnet external to the glass vacuum tube that houses the crystal. The arrows denote the approximate location of the magnet in each frame. In frames (a) and (b) the magnet is ~10 and 15 mm away from the wall of the glass tube and in (c) it is ~35 mm away. In (d) it is in contact with the glass. In all cases the magnets poles are approximately perpendicular to the *z*-axis of the crystal.

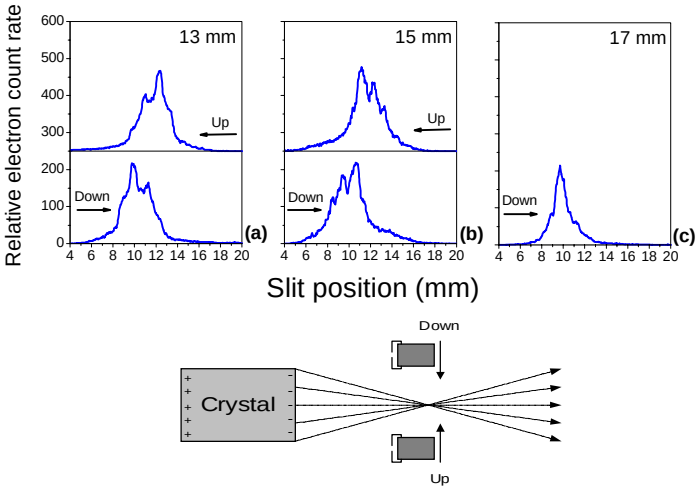

Fig. 29 Results of beam scan to determine if the beam was stable over time and if there was structure in the beam. An arrow indicates the direction of each scan.

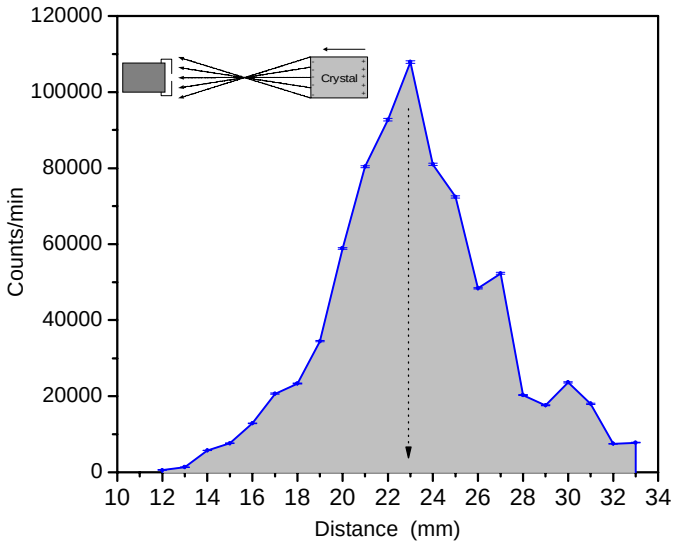

Fig. 30 Results of a beam scan when the detector is moved alone a line that runs through the center of the crystal parallel the z-axis. This was a 4mm in diameter and 10 mm long $LiNbO_3$ crystal.

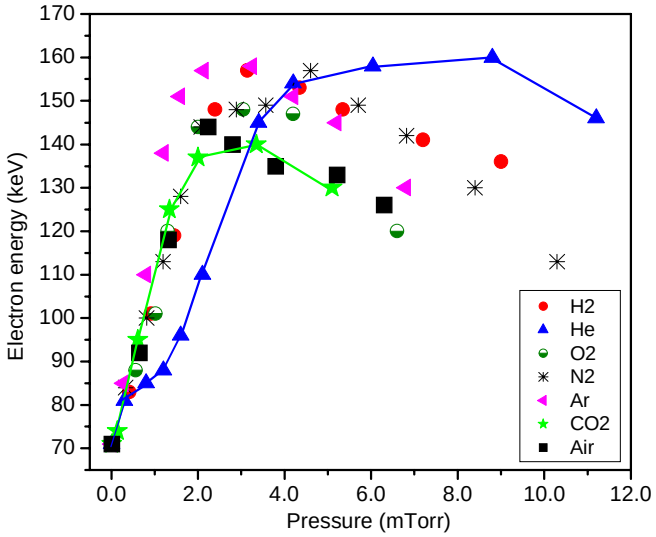

Fig. 31 Maximum electron energy vs. pressure for seven gases. A 4mm diameter by 10mm long $LiNbO_3$ crystal was used. Each data point is the maximum electron energy observed as the crystal cooled from ~180 ^oC at the pressure indicated.

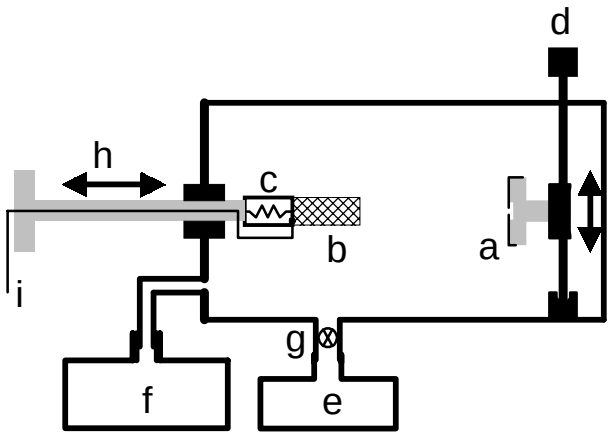

Fig. 32 Schematic diagram of the experimental set-up. (a) 0.1 mm slit and surface barrier detector. (b) Cylindrical detector. (c) 62-ohm resistor. (d) Motor that moves the slit-detector system vertically. (e) Vacuum pump. (f) Gas container. (g) Gas leak valve. (i) Thermocouple and heater wires.

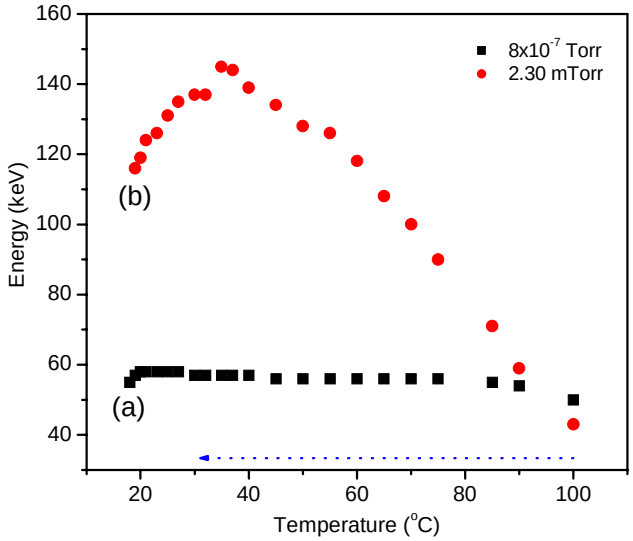

Fig. 33 Shows maximum electron at two pressure (a) there is minimum change in energy as the crystal cooled. (b) There is a significant change in electron energy as the same crystal cools this is gas amplification.

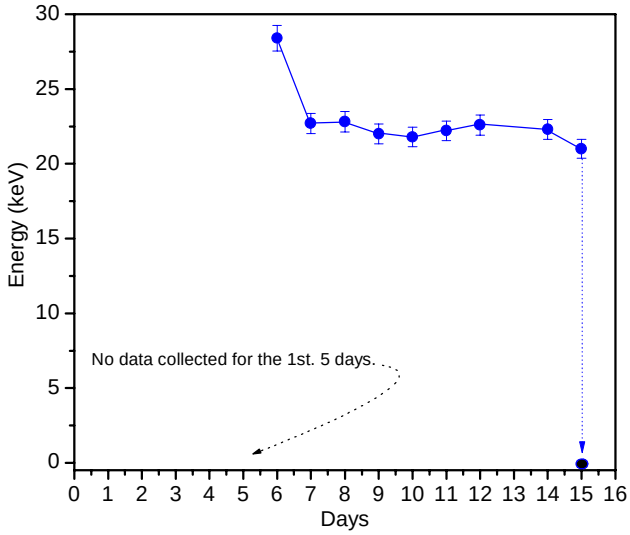

Fig. 34 Electron energy of the first peak on the 5 th. through the 15 th. day fowling a thermal cycle of a 4X10 mm LiNbO3 crystal to 160 ^{o}C in a high vacuum. On the 16 th. day the pressure was raised to ~10^{-2} Torr.

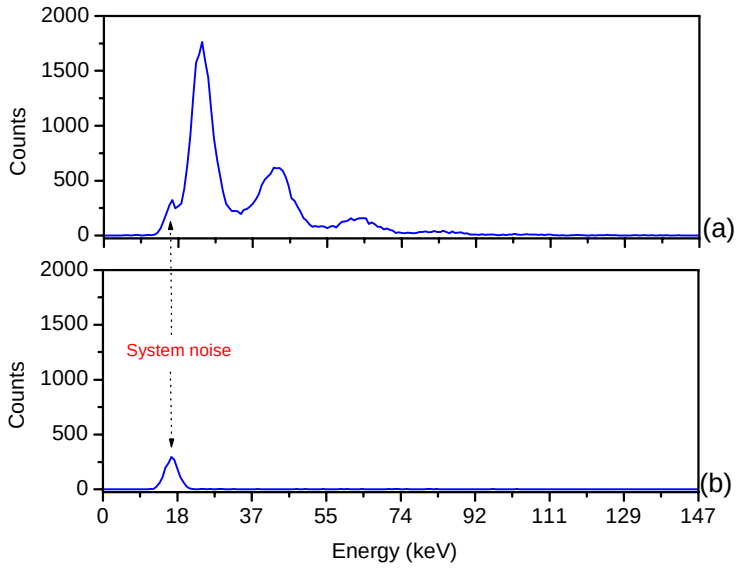

Fig. 35 Electron spectra collected on day 15 fowling the thermal cycle. (a) Spectrum collected just before the pressure was cycled from $3X10^{-6}$ to 10^{-2} to$3X10^{-6}$ Torr. (b) Spectrum taken just after the pressure cycle that permitted the remaining polarization charges to be compensated.

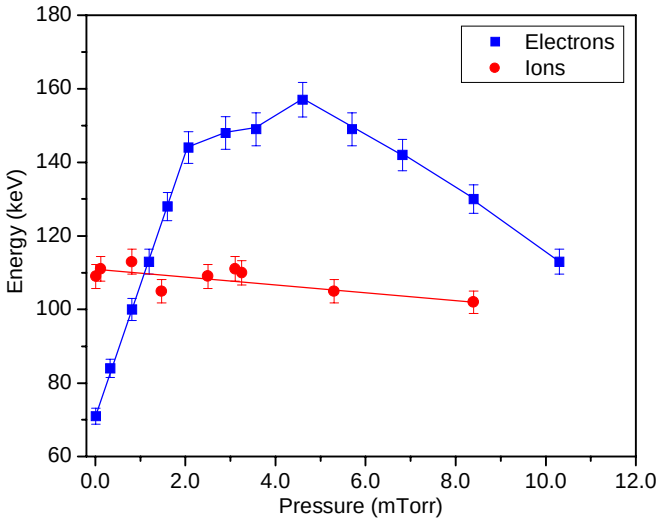

Fig. 36 Shows that there is no gas amplification of ion energy with pressure change in contrast to the situation for electrons. The lines connecting the points are to guide the eye.

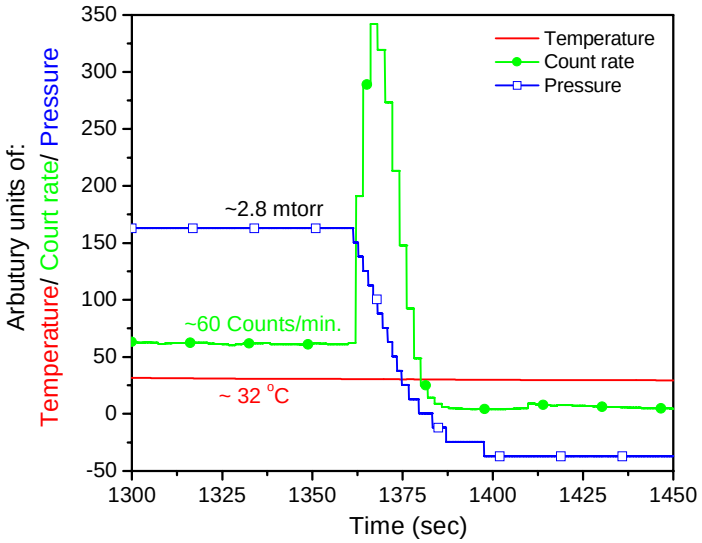

Fig. 37 Shows what happens to the electron count rate when pressure is changed.

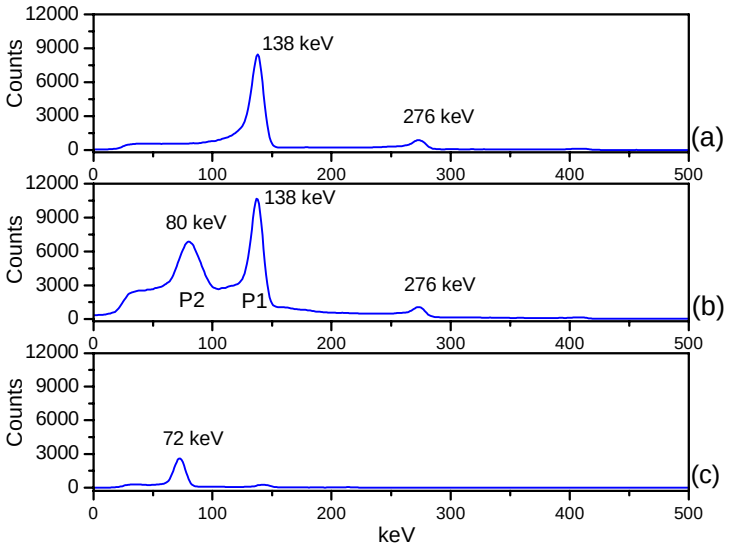

Fig. 38 Electron spectra collected during the period between 1350 and 1400 seconds shown in Fig. Z9. (a) Before a change in pressure. (b) During the change in pressure. (c) After the change in pressure.

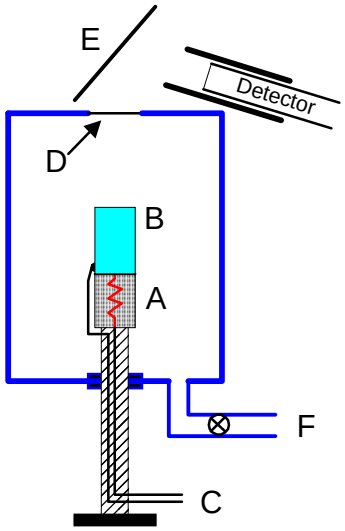

Fig. 39 A thin target D of W/Bi is epoxied to a 2.54 10^{-3} cm Al foil is irradiated by energetic electrons from crystal B on cooling and gives rise to K X-rays and bremsstrahlung. This radiation fluoresces a target at E. The Si/Li detector outside the chamber records the resulting X-ray spectra.

Fig. 40 (a) Bremsstrahlung- fluoresced spectrum of Ta when the geometry is as shown in

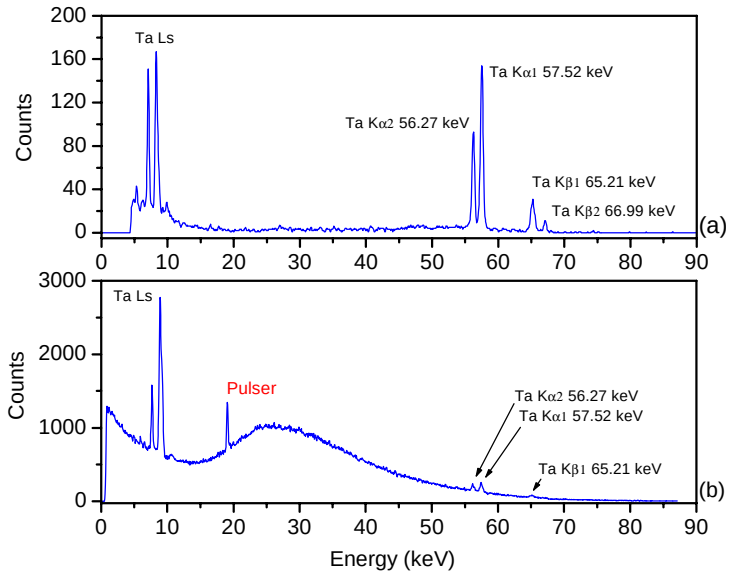

Fig. 40 (a) Bremsstrahlung- fluoresced spectrum of Ta when the geometry is as shown in Fig. 1 and the crystal is $LiNbO_3$. Note the background-free nature of the spectrum. Only one thermal cycles was used and the x-ray detector was only activated when the incident electron energy exceeded the Ta K edge, 67.4 keV. (b) Shows Ta K X-rays superimposed on a bremsstrahlung background when the Ta is irradiated directly by electrons rather than by photons

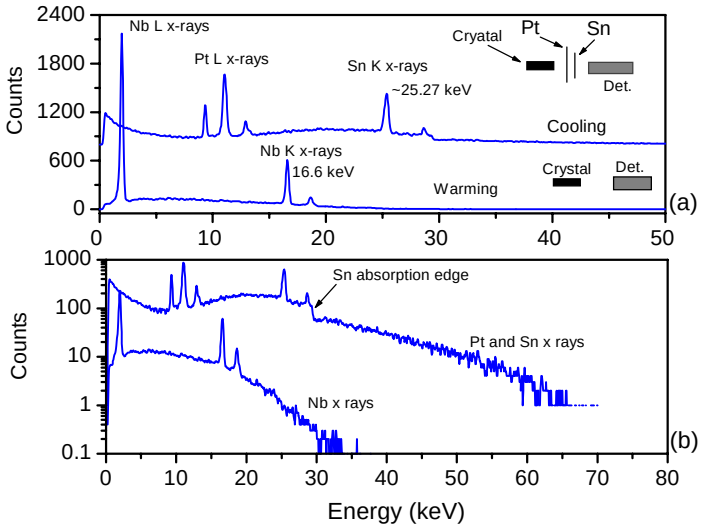

Fig 41 (a) Bremsstrahlung fluoresced Sn K x-rays superimposed on attenuated Bremsstrahlung spectrum arising from electron bombardment of Pt. The crystal was $LiNbO_3$ (5mm long) with its -z base exposed. Note Pt electron excited L x-rays. The geometry is collinear as shown above in the inset. The logarithmic Pt/Sn spectrum in 3(b) is multiplied by an arbitrary number for display purposes. The gas amplification effect is demonstrated since the "cooling" bremsstrahlung maximum energy end point is twice as high as the "heating" end point energy.

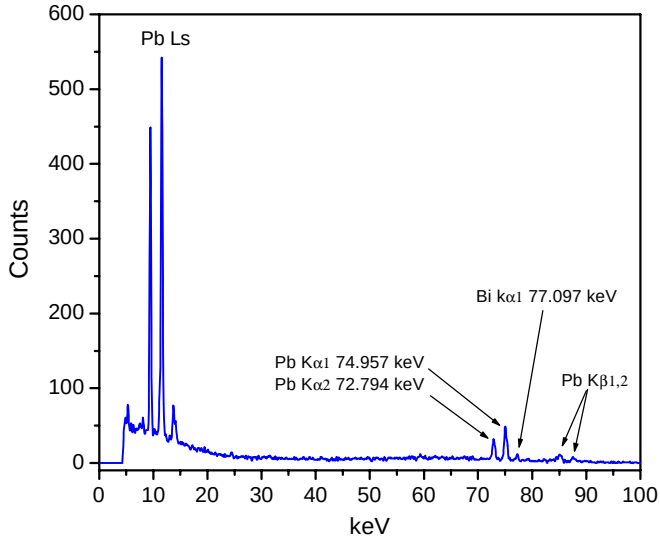

Fig 42 X-ray spectrum of bremsstrahlung fluoresced Pb combined with Bi K x-rays from the target. The geometry was that of Fig. 1 The 10 mm $LiNbO_3$ crystal provided higher energy electrons than the 5 mm $LiTaO_3$ crystal. This spectrum shows that the electron energy was > 90.5 keV, the Bi K-shell ionization energy.

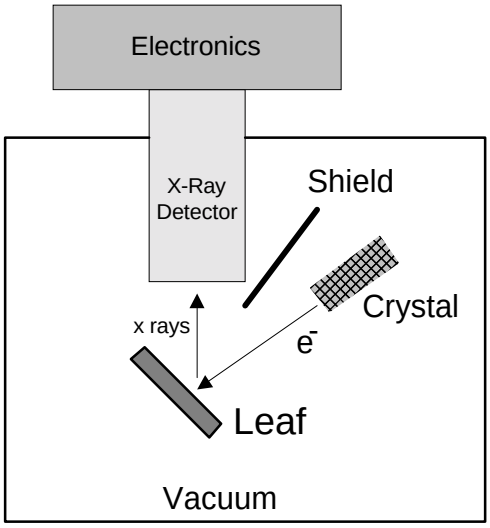

Fig. 43 A schematic diagram of a pyroelectric crystal XRF system.

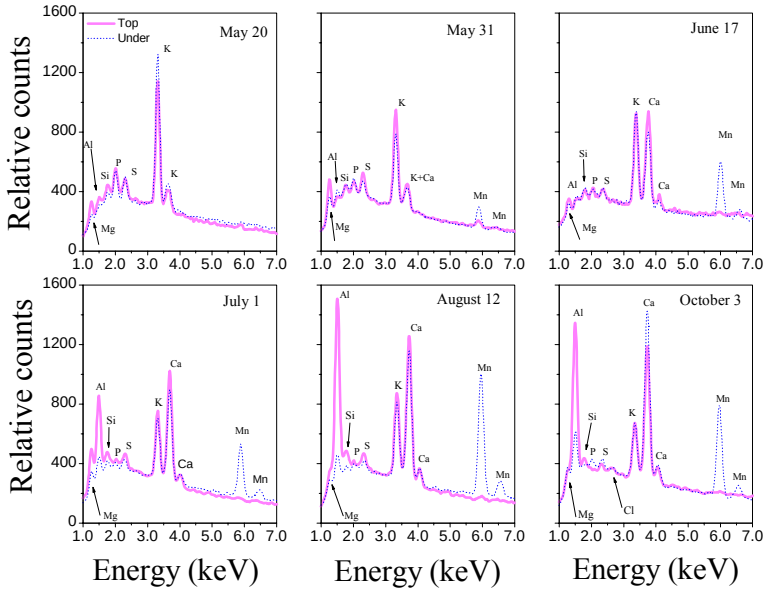

Fig. 44 X-ray spectra of the elements on the top (red) and under side (black) of leaves collected from a pignut hickory. Elements with an atomic number below 12 cannot be detected with the equipment used in this study. Leaves were collected on the date shown in each subfigure. The spectra in each subfigure show the approximate relative concentration of each element in the surface layer of leaves on the tree at the time of collection. When the name of an element appears twice that is a denotation of the K_α and K_β x-rays for that element, the K_α is the larger peak. Note that the K_β of potassium and the K_α of calcium overlap. The K_α, K_β of elements below potassium is not resolved by the equipment used in this study.

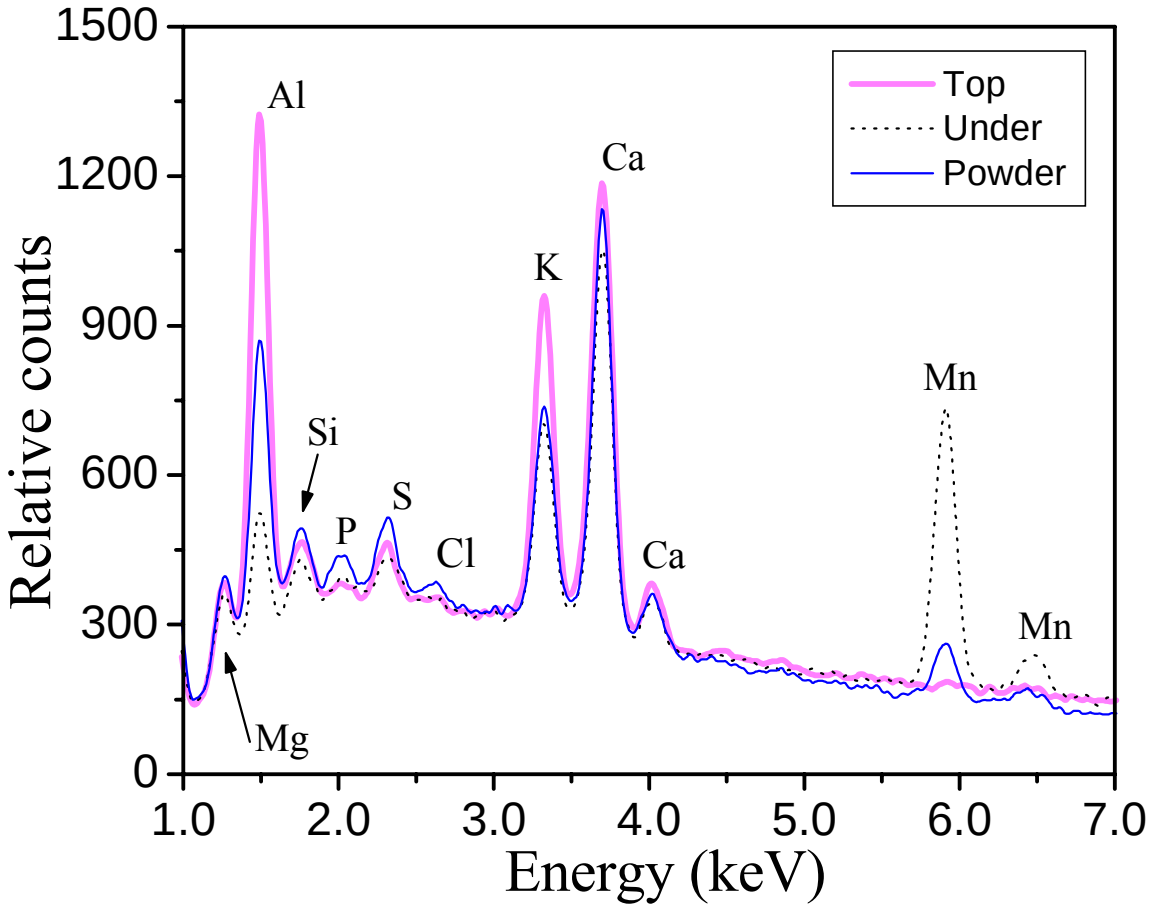

Fig. 45 X-ray spectra of the elements on the top (red) and under side (black) and whole

---

For additional information and other preprints go to:

http://www.binghamton.edu/physics/brownridge.html
http://www.arxiv.org/

http://www.arxiv.org/ftp/cond-mat/papers/0205/0205189.pdf
http://www.arxiv.org/ftp/physics/papers/0107/0107046.pdf
http://www.arxiv.org/ftp/physics/papers/0308/0308093.pdf